Journal of Computational Mathematics
Vol.29, No.5, 2011, 543–573.

http://www.global-sci.org/jcm
doi:10.4208/jcm.1106-m3406

A NUMERICAL BOUNDARY EIGENVALUE PROBLEM FOR ELASTIC CRACKS IN FREE AND HALF SPACE*

Darko Volkov
Department of Mathematical Sciences, Worcester Polytechnic Institute, Worcester MA 01609, USA
Email: darko@wpi.edu

Abstract

We present in this paper a numerical method for hypersingular boundary integral equations. This method was developed for planar crack problems: additional edge singularities are known to develop in that case. This paper includes a rigorous error analysis proving the convergence of our numerical scheme. Three types of examples are covered: the Laplace equation in free space, the linear elasticity equation in free space, and in half space.

Mathematics subject classification: 45L05, 65R20, 86-08.
Key words: Hypersingular boundary integral equations, Numerical error analysis, Eigenvalue problems, Faults in free space and half space, Somigliana tensor of the second kind in free space and in half space.

1. Introduction

1.1. The three types of boundary eigenvalue problems studied in this paper

In this paper we study three types of numerical eigenvalue problems using hypersingular boundary integral equations on cracks, either in three dimensional space, or in the lower half space with traction free boundary conditions on the top plane $x_3 = 0$. The first type of problem involves the scalar Laplace operator in free space, cut by a planar fault Γ. Due to the possibility of changing coordinates by rotation and translation we will assume that Γ is contained in the plane $x_3 = 0$. Denoting e_1, e_2, e_3, the natural basis for $\mathbb{R}^3$, we choose the normal vector for Γ to be $n = -e_3$.

We seek to evaluate eigenfunctions f defined in some adequate functional space, ensuring decay at infinity, and satisfying

$$\Delta f = 0, \qquad \text{in } \mathbb{R}^3 \setminus \Gamma, \tag{1.1a}$$

$$[\partial_n f] = 0, \qquad \text{across } \Gamma, \tag{1.1b}$$

$$\partial_n f = \gamma [f]. \tag{1.1c}$$

Here γ is the eigenvalue and brackets indicate jumps across Γ, namely

$$[\partial_n f] = \lim_{(x_1,x_2)\in\Gamma,\, x_3\to 0^+} \partial_n f(x_1, x_2, x_3) - \partial_n f(x_1, x_2, -x_3), \quad (x_1, x_2, 0) \in \Gamma.$$

A two dimensional analog to this eigenvalue problem was shown to be relevant to the study of the destabilization of strike slip faults: see [3] and [7]. We are not aware of a straightforward physical interpretation of problem (1.1) in 3D. In the present study this problem is a convenient

* Received May 10, 2010 / Revised version received December 14, 2010 / Accepted February 25, 2011 / Published online September 9, 2011 /

intermediate step between the strike slip case and the fully three dimensional elasticity case. In particular this step is instrumental in comparing our numerical method to others and in deriving an error analysis which is also expected to hold in the subsequent two cases.

The second type of eigenvalue problem considered in this paper involves linear elasticity in free space. The unknown eigenfunctions to be found are vector fields defined in some adequate functional space, ensuring some decay at infinity, and satisfying

$$\mu\Delta\varphi + (\lambda+\mu)\nabla\mathrm{div}\,\varphi = 0, \qquad \text{in } \mathbb{R}^3 \setminus \Gamma, \tag{1.2a}$$

$$[\varphi\cdot e_3] = 0,\ [\varphi\cdot e_2] = 0,\ [T_n\varphi] = 0, \qquad \text{across } \Gamma, \tag{1.2b}$$

$$T_n\varphi\cdot e_1 = \beta[\varphi]\cdot e_1, \tag{1.2c}$$

where the assumptions on Γ are the same as previously, β is the eigenvalue, and $T_n\varphi$ is the usual notation for the stress vector, that is,

$$\sum_{j=1}^{3}(\lambda\,\mathrm{div}\,\varphi\,\delta_{ij} + \mu(\partial_i\varphi_j + \partial_j\varphi_i))n_j.$$

Eqs. (1.2) model a fault in free elastic space undergoing destabilization during which slip (that is, displacement discontinuities) is allowed only in the e_1 direction. A thorough study of this eigenvalue problem, including a formal proof for simplicity of the first eigenspace, was undertaken in [19]. The numerical results shown in that paper are, however, limited by the fact that they were produced by a finite element software package. Questions of numerical convergence, error analysis, and computational domain truncation, were all left unanswered: we propose to address them in this present paper.

The third type of eigenvalue problem considered in this paper involves linear elasticity in half space. Denote $\mathbb{R}^{3-}$ the open set of points (x_1, x_2, x_3) in $\mathbb{R}^3$ such that $x_3 < 0$. We assume that the fault Γ is strictly included in $\mathbb{R}^{3-}$. Traction free conditions are imposed on the top boundary $x_3 = 0$. These conditions are relevant to applications in geophysics. By rotation we can assume that the plane containing Γ has normal direction $n = (n_1, 0, n_3)$. Let t_1 and t_2 be two vectors such that (n, t_1, t_2) forms an orthonormal basis for $\mathbb{R}^3$. The unknown eigenfunctions to be found are vector fields defined in some adequate functional space, ensuring some decay at infinity, and satisfying

$$\mu\Delta\psi + (\lambda+\mu)\nabla\mathrm{div}\,\psi = 0, \qquad \text{in } \mathbb{R}^{3-} \setminus \Gamma, \tag{1.3a}$$

$$T_n\psi = 0, \qquad \text{on } x_3 = 0 \tag{1.3b}$$

$$[\psi\cdot n] = 0,\ [\psi\cdot t_2] = 0,\ [T_n\psi] = 0, \qquad \text{across } \Gamma, \tag{1.3c}$$

$$T_n\psi\cdot t_1 = \beta[\psi\cdot t_1]. \tag{1.3d}$$

Eqs. (1.3) model a fault in free elastic half space undergoing destabilization during which slip (that is displacement discontinuities) is allowed only in the t_1 direction. No forces are applied on the top boundary $x_3 = 0$.

1.2. Outline of our main results and overview of alternative computational methods found in the literature

The main achievement of this paper is to provide a numerical method for each of the problems (1.1), (1.2), (1.3) which relies on boundary integral formulations. The advantage of

this kind of formulation is twofold: firstly it leads to linear systems of reduced size; secondly conditions at infinity are naturally embedded in the choice of an adequate Green's function. This second advantage is particularly important for the half space problem (1.3). Of course we had to contend with some difficulties inherent to boundary integral equations. One particular challenge pertains to the hypersingularities of the associated integral operator: in the present case these are singularities of order $\mathcal{O}(r^{-3})$ for diagonal points. In this sense these operators can be interpreted as being both integral and differential. A second challenge pertains to the fact that solutions to (1.1), or (1.2), or (1.3), must have square root type singularities on $\partial\Gamma$, the edge of the crack. These singularities and related Sobolev regularity results were studied by Stephan and Wendland in [21] and [15].

It is noteworthy that hypersingular boundary integral equations on *closed* surfaces are substantially easier to solve numerically: one can employ fast and accurate quadratures, see for example the work by Ying *et al.*, [22]. Loosely speaking, the main difficulty arising in our study, which involves hypersingular boundary integral equations on *open* surfaces, lies in the competition between hypersingularities due to the Green's integral operator and the square root singularities due to the edge $\partial\Gamma$ of the crack. For instance the high order quadrature methods employed in [22] would fail in our case since derivatives of the solution blow up near $\partial\Gamma$. Furthermore clustering points near $\partial\Gamma$ proves to be ineffective because of the integral and differential nature of the Green's integral operator: clustering can improve numerical integration but since derivatives are unbounded near the edge $\partial\Gamma$, there is no overall gain in accuracy; even worse, conditioning deteriorates.

In case of a special geometry for the fault Γ it is conceivable that an astute change of variables combined to the use of special quadrature rules will produce a very efficient and fast numerical method. Such was the case in a paper by Dascalu *et al.*, see [3], for the two dimensional analog to (1.1): the crack studied in that paper is just the line segment $[-1,1]\times\{0\}$ in $\mathbb{R}^2$ and special Chebychev points of the second kind were put to use. In contrast we focus in this paper on finding a method applicable to general geometries for cracks Γ: we only require Γ to be planar and some smoothness for the edge $\partial\Gamma$. An early review paper by Martin *et al.*, [10], lists the hurdles in the way of developing efficient numerical methods for crack problems in 3D, discusses various solution methods, and recommends using piecewise linear approximations combined to additional square root terms near the edge of the crack. Later, finite element boundary methods for crack problems in 3D were designed, see [16]. More sophisticated studies of crack problems in 3D have since been undertaken, with a particular emphasis on dynamic unstable evolution. Badea *et al.*, [2], use spatial finite elements while Aochi *et al.*, [1], rely on boundary integral methods. Note that these two studies do not include any error analysis and are limited to the free space case.

Ultimately the boundary integral equation method introduced in this paper is proved, in case of problem (1.1), to be at least $\mathcal{O}(h^{\frac{2}{3}}\ln h)$ accurate for about $\mathcal{O}(n^2)$ interpolation points placed on Γ, and where $h=\mathcal{O}(n^{-1})$. In effect a convergence rate of $\mathcal{O}(h\ln h)$ is observed for each of the eigenfunction problems (1.1), (1.2), and (1.3). Although this convergence rate might seem quite modest, it is in fact competitive in comparison to existing methods. For instance, a paper on a new finite element method for a mixed boundary value problem for 3D elasticity by Hsiao and Wendland [6], features a method of order $\mathcal{O}(h^{\delta})$ where δ is a constant in $(0,\frac{1}{2})$.

Finally let us make a remark on computational speed for our proposed integral equation method. In the case of problem (1.1) most of the computational time is spent on evaluating the coefficients of the matrix for the discretized problem. Assume now that n, a parameter

introduced in the next section quantifying the fineness of the discretization, is fixed. Denote S the square $[-1,1]\times[-1,1]$. We can then first compute the coefficients of the matrix M_S for the discretized problem in the case $\Gamma = S$; from there for any other geometry Γ, we can assume by translation and dilation that Γ is included in S. We will explain how the coefficients of the matrix M_Γ for the discretized problem relative to Γ, can just be sampled from the matrix M_S. Finding the lowest eigenvalue for M_Γ typically takes under one second. A similar remark can be made for problem (1.2), assuming that λ and μ are fixed. Remarkably, setting $\lambda = \mu = 1$ is a common modeling choice in geophysical applications . The computation then depends only on the geometry of Γ; our computational scheme is very fast in that case. This method could be quite useful in practice to inverse problems for the reconstruction of the geometry of Γ.

Our paper will unfold as follows: Section 2 is devoted to the scalar eigenvalue problem (1.1). We explain in detail the theoretical foundations of our numerical method in Section 2.1, and we perform a rigorous error analysis in 2.2. The minutia of this implementation as well as the error analysis both hold in the other two cases covered in this paper, up to appropriate adjustments, and will not be repeated. In Section 2.3 we verify our numerical scheme by comparison to a hypersingular integral whose exact value is known. In Section 2.4 we provide numerical results for Eq. (1.1) first using a finite element package and then applying our integral equation method. This section demonstrates that while the two sets of estimates for the eigenvalue γ are comparable, we are more confident of our integral equation method due to clearer convergence behavior and better conditioning. It will also become clear in Section 2 why once the matrix for discretizing the boundary integral operator relative to Eq. (1.1), where Γ is the unit square, is tabulated, we can henceforth make very rapid computations of eigenvectors for any other smooth and planar geometry for Γ.

Section 3 is devoted to cracks in free space whose unstable quasi static evolution is modeled by Eq. (1.2). In Section 3.1 we explain how the numerical method introduced in Section 2 can be adjusted to handle Eq. (1.2). We present in Section 3.2 numerical outputs relative to equations (1.2) resulting from, first a finite element package, and second, our integral equation method. Section 4 is devoted to half space elasticity, which is the most interesting case for applications to geophysics. After introducing governing equations, we comment on the derivation of the Green's tensor for that case, with an emphasis on singular points. We then show numerical results for a calculation involving a fault whose tip is very close to the top surface. Note that a standard finite element package is inadequate for such cases due to the additional numerical difficulties related to near surface points. Finally, we show a numerical illustration of convergence of eigenvectors for the half space problem (1.2) to the free space problem (1.3) as the fault depth grows large. In the last section we summarize our findings and point to further problems of interest which we intend to study in the future.

2. The Laplace Eigenvalue Problem for a Crack in Free Space

We first introduce an adequate functional space where problem (1.1) is well posed. We define the functional space $\mathcal{L}$ to be the closure for the norm $(\int_{\mathbb{R}^3}|\nabla u|^2)^{\frac{1}{2}}$ of the space of scalar functions in $H^1(\mathbb{R}^3\setminus\overline{\Gamma})$ with bounded support. $\mathcal{L}$ is used to reframe eigenvalue problem (1.1)

as follows, find f in $\mathcal{L}$ and a real number γ, such that,

$$\Delta f = 0, \qquad \text{in } \mathbb{R}^3 \setminus \Gamma, \tag{2.1a}$$

$$[\partial_n f] = 0, \qquad \text{across } \Gamma, \tag{2.1b}$$

$$\partial_n f = \gamma[f]. \tag{2.1c}$$

Solving the PDE (2.1) is equivalent to minimizing

$$\frac{\int_{\mathbb{R}^3} |\nabla f|^2}{\int_\Gamma [f]^2}, \quad f \in \mathcal{L},\ [f] \neq 0,$$

see [19]. By translation, rotation, and dilation we can assume without loss of generality that the crack Γ is included in the square $[-1,1] \times [-1,1]$, which we denote S. We will use the free space Green's function for the Laplacian,

$$G(x,y) = \frac{1}{4\pi} \frac{1}{|x-y|}.$$

If f solves (2.1) then the following relation holds for x in Γ

$$\gamma[f(x)] = -\partial_{n(x)} \int_\Gamma \partial_{n(y)} G(x,y)[f(y)]dy. \tag{2.2}$$

For x and y on Γ we set

$$N(x,y) = -\partial_{n(x)}\partial_{n(y)} G(x,y), \quad u(x) = [f(x)].$$

Note that if $x \neq y$, and x and y are in the plane of equation $x_3 = 0$, $N(x,y) = -\frac{1}{4\pi}|x-y|^{-3}$. Eq. (2.2) can be rewritten as

$$\gamma\, u(x) = \int_\Gamma N(x,y)\, u(y)dy, \tag{2.3}$$

where the unknown eigenvector u is in $\tilde{H}^{\frac{1}{2}}(\Gamma)^2$ and the integral is understood in the hypersingular sense, see [15]. In the present planar case $\tilde{H}^{\frac{1}{2}}(\Gamma)^2$ is the space of vector fields in Γ such that if extended by zero to $\mathbb{R}^2$, they become elements of the space $H^{\frac{1}{2}}(\mathbb{R})^2$.

2.1. The numerical method

We start this section by recalling results on the existence of a first eigenvector solving equation (2.3) and stating its regularity properties. We know from [15] that we can define a linear operator $\mathcal{N}$ from $\tilde{H}^{\frac{1}{2}}(\Gamma)^2$ to $H^{-\frac{1}{2}}(\Gamma)^2$ by setting for u in $\tilde{H}^{\frac{1}{2}}(\Gamma)^2$

$$\mathcal{N}u(x) = \int_\Gamma N(x,y)\, u(y)dy.$$

According to [21] $\mathcal{N}$ is bijective and continuous. Defining $\mathcal{I}_1$ the natural injection from $L^2(\Gamma)^2$ to $H^{-\frac{1}{2}}(\Gamma)^2$ and $\mathcal{I}_2$ the natural injection from $\tilde{H}^{\frac{1}{2}}(\Gamma)^2$ to $L^2(\Gamma)^2$, $\mathcal{M} = \mathcal{I}_2\mathcal{N}^{-1}\mathcal{I}_1$ is a positive definite compact and symmetric linear mapping. Therefore it has a largest eigenvalue. The corresponding eigenspace is known to be one dimensional, see [19]. In this section we will denote

$$\gamma_1 \text{ the smallest eigenvalue of } \mathcal{N},\ u_1 \text{ an associated eigenvector such that } \int_\Gamma u_1^2 = 1 \tag{2.4}$$

In other words the pair u_1, γ_1 satisfies (2.3) and γ_1 is minimal for that condition. We also know from [21] that although eigenvectors are smooth in Γ, they tend to zero near the edge $\partial\Gamma$ while having square root singularities. A solution u to (2.3) can be extended to S by setting it equal to zero in $S \setminus \Gamma$. The extended function, which we will still denote u for convenience, is in the Sobolev space $H_0^{\frac{1}{2}}(S)^2$, if $\overline{\Gamma}$ is strictly included in S, see [15].

Define W to be the set $S \setminus \partial\Gamma$. Our numerical method consists of determining approximations in the space of three times continuously differentiable functions in W, $C^3(W)$, to solutions u of (2.3). These approximations are done on a lattice of points. Of course the derivatives of u grow large near $\partial\Gamma$. We introduce a smooth function d defined on Γ equal to the distance from x to $\partial\Gamma$ if x is close enough to $\partial\Gamma$; if x is far enough from $\partial\Gamma$ $d(x)$ is set to be equal to 1, and in between these two regions d is positive and smooth. This is possible since the distance from x to $\partial\Gamma$ is well defined and smooth in a small tubular neighborhood of $\partial\Gamma$. We will consider functions u is such that there is a positive constant A such that for all x in Γ

$$|D^\alpha u(x)| \leq A d(x)^{\frac{1}{2}-|\alpha|}, \quad 0 \leq |\alpha| \leq 3. \tag{2.5}$$

According to [21] solutions to eigenvalue problem (2.3) satisfy the singularity condition (2.5).

Our numerical method takes advantage of the fact that for a fixed interior point x of Γ (relative to the topology of the plane $x_3 = 0$), a solution u to (2.3) is smooth in a neighborhood of x. We may then remove singularities by Taylor expansions of order 2. Singularity removal is a rather common technique for integral equations, however, it is usually employed for logarithmic or Cauchy type singularities. For stronger singularities there is a fair amount of literature in the case of 2D problems, including some work by the author of the present paper, see [7]. The case of 3D problems is substantially more challenging, since the geometry of the crack must be approximated, and the integrand does not become infinitely smooth after singularity removal, as noted below.

Our method is based on the following decomposition for x in Γ:

$$\begin{aligned}
&\int_\Gamma N(x,y)u(y)dy = \int_S N(x,y)u(y)dy \\
&= \int_S N(x,y)U(y)dy + u(x)\int_S N(x,y)dy + \sum_{i=1}^{2} \partial_i u(x) \int_S (y_i - x_i)N(x,y)dy \\
&\qquad + \frac{1}{2}\sum_{i=1}^{2}\sum_{j=1}^{2} \partial_i\partial_j u(x) \int_S (y_i - x_i)(y_j - x_j)N(x,y)dy,
\end{aligned} \tag{2.6}$$

where the function U is defined by

$$U(y) = u(y) - u(x) - \sum_{i=1}^{2} \partial_i u(x)(y_i - x_i) - \frac{1}{2}\sum_{i=1}^{2}\sum_{j=1}^{2} \partial_i\partial_j u(x)(y_i - x_i)(y_j - x_j). \tag{2.7}$$

Note that U is merely a quadratic function of y in $S \setminus \Gamma$. In addition note that the six integrals

$$\begin{aligned}
&I^0 := \int_S N(x,y)dy, \qquad I_i^1 := \int_S (y_i - x_i)N(x,y)dy, \\
&I_{i,j}^2 := \int_S (y_i - x_i)(y_j - x_j)N(x,y)dy,
\end{aligned} \tag{2.8}$$

have to be understood in the following sense: let $x = (x_1, x_2)$ be in Γ and $\mathbf{x} = (x_1, x_2, x_3)$ be in $\mathbb{R}^3$. Then

$$I^0 := -\lim_{x_3 \to 0} \int_S \partial_{n(x)} \partial_{n(y)} G(\mathbf{x}, y) dy, \qquad I_i^1 := -\lim_{x_3 \to 0} \int_S (y_i - x_i) \partial_{n(x)} \partial_{n(y)} G(\mathbf{x}, y) dy,$$
$$I_{i,j}^2 := -\lim_{x_3 \to 0} \int_S (y_i - x_i)(y_j - x_j) \partial_{n(x)} \partial_{n(y)} G(\mathbf{x}, y) dy. \tag{2.9}$$

These six integrals and limits can be evaluated in closed form. Formulas are provided in the Appendix.

The derivatives of u will have to be approximated numerically. Let n be a positive integer and $h = 2/n$. We introduce the collocation points $x_{ij} := (-1 + ih, -1 + jh)$ and the grids of points

$$S_n := \{x_{ij} : 1 \le i, j \le n - 1\}, \qquad \Gamma_n := \{x \in S_n \cap \Gamma : d(x) \ge h\}. \tag{2.10}$$

We denote

$$\widetilde{\partial_i u}(x) = \frac{u(x + he_i) - u(x - he_i)}{2h}, \quad \widetilde{\partial_i \partial_i u}(x) = \frac{u(x + he_i) + u(x - he_i) - 2u(x)}{h^2}, \tag{2.11}$$
$$\widetilde{\partial_i \partial_j u}(x) = \frac{u(x + he_i + he_j) + u(x - he_i - hej) - u(x + he_i - he_j) - u(x - he_i + he_j)}{2h^2}, \tag{2.12}$$

and we define $\tilde{U}$ the following discrete approximation to U,

$$\tilde{U}(y) = u(y) - u(x) - \sum_{i=1}^{2} \widetilde{\partial_i u}(x)(y_i - x_i) - \frac{1}{2} \sum_{i=1}^{2} \sum_{j=1}^{2} \widetilde{\partial_i \partial_j u}(x)(y_i - x_i)(y_j - x_j). \tag{2.13}$$

Expression (2.6) seems to be relevant for analyzing the operator $\mathcal{N}$. However another form is more adequate for performing a numerical analysis of a method derived from (2.6). Introduce a function $\tilde{V}$ which will serve as a convenient intermediate between U and $\tilde{U}$

$$\tilde{V}(y) = u(y) - u(x) - \sum_{i=1}^{2} \partial_i u(x)(y_i - x_i) - \frac{1}{2} \sum_{i=1}^{2} \sum_{j=1}^{2} \widetilde{\partial_i \partial_j u}(x)(y_i - x_i)(y_j - x_j), \tag{2.14}$$

and apply the following decomposition for x in Γ:

$$\int_\Gamma N(x, y) u(y) dy = \int_S N(x, y) u(y) dy$$
$$= \int_S N(x, y) \tilde{V}(y) dy + u(x) \int_S N(x, y) dy + \sum_{i=1}^{2} \partial_i u(x) \int_S (y_i - x_i) N(x, y) dy$$
$$+ \frac{1}{2} \sum_{i=1}^{2} \sum_{j=1}^{2} \widetilde{\partial_i \partial_j u}(x) \int_S (y_i - x_i)(y_j - x_j) N(x, y) dy. \tag{2.15}$$

Note that the integral $\int_S N(x, y) \tilde{V}(y) dy$ can be understood as an integral in the Lebesgue space $L^1(S)$ since

$$\tilde{V}(y) = \mathcal{O}(|x - y|^2), \quad N(x, y) = \mathcal{O}(|x - y|^{-3}).$$

We then derive the discrete operator $\tilde{N}$ from the right hand side expression (2.15),

$$\tilde{N} u(x) = \sum_{y \in S_n,\, y \ne x} N(x, y) \tilde{U}(y) h^2 + u(x) I^0 + \sum_{i=1}^{2} \widetilde{\partial_i u}(x) I_i^1 + \frac{1}{2} \sum_{i=1}^{2} \sum_{j=1}^{2} \widetilde{\partial_i \partial_j u}(x) I_{i,j}^2. \tag{2.16}$$

2.2. Error analysis

2.2.1. Estimates for the finite differences approximating the derivatives of u

By application of Taylor's formula we find that for x in Γ_n

$$\widetilde{\partial_i u}(x) - \partial_i u(x) = \mathcal{O}(Ahd(x)^{-\frac{3}{2}}), \quad \widetilde{\partial_i \partial_j u}(x) - \partial_i \partial_j u(x) = \mathcal{O}(Ahd(x)^{-\frac{5}{2}}). \tag{2.17}$$

Since our schemes for first derivatives is order 2 accurate we have the higher order estimate

$$\widetilde{\partial_i u}(x) - \partial_i u(x) = \mathcal{O}(Ah^2 d(x)^{-\frac{5}{2}}). \tag{2.18}$$

The following estimate, which does not depend on h, will also be needed

$$\widetilde{\partial_i \partial_i u}(x) = \mathcal{O}(Ad(x)^{-\frac{3}{2}}). \tag{2.19}$$

2.2.2. Interior estimates

In this section we estimate the difference between the discrete sum and finite differences (2.16) and the continuous integrals and derivatives given by (2.15), if x is in Γ_n and remains bounded away from the edge $\partial\Gamma$. In effect we assume that

$$d(x) \geq B, \tag{2.20}$$

where the positive constant B depends only on the geometry of Γ and will be specified later. Let S_{ij} be the square $x_{ij} + [-\frac{h}{2}, \frac{h}{2}] \times [-\frac{h}{2}, \frac{h}{2}]$, f a function of class C^1 on S_{ij}. Due to Taylor's formula centered at x_{ij},

$$\left| \int_{S_{ij}} f(x)dx - h^2 f(x_{ij}) \right| \leq h^3 \max_{S_{ij}} |\nabla f|, \tag{2.21}$$

where $\max_{S_{ij}} |\nabla f|$ is the maximum of the first derivatives of f over S_{ij}.
We separate two cases defined according to the position of y relative to x. Γ_n. Let D be a positive constant smaller than $\frac{B}{2}$.

Case 1: $|x - y| \geq D$

For some constant C independent of u and Γ the following holds

$$|\nabla(N(x,y)\tilde{V}(y))| \leq CD^{-3}|\nabla \tilde{V}(y)| + CD^{-4}|\tilde{V}(y)|.$$

Now due to (2.5)

$$|\tilde{V}(y)| \leq Ad(y)^{\frac{1}{2}} 1_\Gamma(y) + CAB^{-\frac{3}{2}},$$
$$|\nabla \tilde{V}(y)| \leq Ad(y)^{-\frac{1}{2}} 1_\Gamma(y) + CAB^{-\frac{3}{2}},$$

thus the difference

$$\int_{y \in S,\, D \leq |y-x|} N(x,y)\tilde{V}(y)dy - \sum_{y \in S_n,\, D \leq |y-x|} N(x,y)\tilde{V}(y)h^2, \tag{2.22}$$

which is less than

$$\sum_{y_{ij} \in \Gamma_n, D \leq |y_{ij}-x|} \int_{S_{ij}} N(x,y)\tilde{V}(y) - h^2 N(x,y_{ij})\tilde{V}(y_{ij})\, dy$$

is, according to (2.21), less than

$$\sum_{y\in S_n} h^3 d(y)^{-\frac{1}{2}} AB^{-\frac{3}{2}} D^{-4} \le ChAB^{-\frac{3}{2}} D^{-4} \int_0^1 s^{-\frac{1}{2}} ds = ChAB^{-\frac{3}{2}} D^{-4},$$

for some positive constant C.

We now need to estimate the difference

$$\sum_{y\in S_n,\, D\le|y-x|} N(x,y)\tilde{U}(y)h^2 \quad - \sum_{y\in S_n,\, D\le|y-x|} N(x,y)\tilde{V}(y)h^2.$$

Since

$$|\tilde{U}(y)-\tilde{V}(y)| = \left|\sum_{i=1}^{2}(\partial_i u(x) - \widetilde{\partial_i u}(x))(y_i - x_i)\right| \le CAhd(x)^{-\frac{3}{2}},$$

we have that

$$\left|\sum_{y\in S_n,\, D\le|y-x|} N(x,y)\tilde{U}(y)h^2 \quad - \sum_{y\in S_n,\, D\le|y-x|} N(x,y)\tilde{V}(y)h^2\right| \le CAhB^{-\frac{3}{2}}.$$

We have thus proved that

$$\left|\int_{y\in S,\, D\le|y-x|} N(x,y)\tilde{V}(y)dy \quad - \sum_{y\in S_n,\, D\le|y-x|} N(x,y)\tilde{V}(y)h^2\right| \le ChAB^{-\frac{3}{2}} D^{-4}.$$

Case 2: y is near x: $|x-y| \le D$

We make the following observation: setting $\rho = |x-y|$, as ρ approaches zero, for U defined on (2.7)

$$|U(y)| \le CAd(x)^{-\frac{5}{2}}\rho^3 \le CAB^{-\frac{5}{2}}\rho^3,$$

after simplifying $U(y) - \tilde{V}(y)$ we find that

$$|U(y)-\tilde{V}(y)| \le ChAd(x)^{-\frac{5}{2}}\rho^2 \le ChAB^{-\frac{5}{2}}\rho^2,$$

so that

$$|\tilde{V}(y)| \le ChAB^{-\frac{5}{2}}\rho^2 + CAB^{-\frac{5}{2}}\rho^3.$$

A similar process will show that

$$|\nabla\tilde{V}(y)| \le ChAB^{-\frac{5}{2}}\rho + CAB^{-\frac{5}{2}}\rho^2.$$

Since $|N(x,y)| \le C\rho^{-3}$ and $|\nabla_y N(x,y)| \le C\rho^{-4}$ we can now apply (2.21) to claim that the difference

$$\int_{y\in S,\, 0<|y-x|<D} N(x,y)\tilde{V}(y)dy \quad - \sum_{y\in S_n, 0<|y-x|<D} N(x,y)\tilde{V}(y)h^2 \tag{2.23}$$

is, of order

$$\sum_{y\in S_n,\, h\le|y-x|<D} CAB^{-\frac{5}{2}}(h^4\rho^{-2} + h^3\rho^{-1}) \le ChAB^{-\frac{5}{2}}\left(h\int_h^D \rho^{-1}d\rho + \int_h^D d\rho\right) \le ChAB^{-\frac{7}{2}}.$$

We now note that

$$\tilde{V}(y) - \tilde{U}(y) = -\sum_{i=1}^{2} \left(\partial_i u(x) - \widetilde{\partial_i u}(x)\right)(y_i - x_i),$$

so that using (2.18)

$$\left|\tilde{V}(y) - \tilde{U}(y)\right| \leq Ah^2 d(x)^{-\frac{5}{2}}\rho \leq Ah^2 B^{-\frac{5}{2}}\rho.$$

Then the difference

$$\sum_{y\in S_n, 0<|y-x|<D} N(x,y)\left(\tilde{V}(y) - \tilde{U}(y)\right)h^2$$

is of order

$$\sum_{y\in S_n,\, h\leq|y-x|<D} CAh^4 B^{-\frac{5}{2}}\rho^{-2} \sim CAh^2 B^{-\frac{5}{2}}\int_h^C \rho^{-2}\rho d\rho \leq CAhB^{-\frac{5}{2}}.$$

We can now combine the outcomes from the two previous cases to conclude that if $d(x) \geq B$ then

$$\begin{aligned}\left|\int_{y\in S,\, 0<|y-x|<C} N(x,y)\tilde{V}(y)dy \quad - \sum_{y\in S_n, 0<|y-x|<C} N(x,y)\tilde{U}(y)h^2\right| \\ \leq CAh\left(B^{-\frac{5}{2}} + B^{-\frac{3}{2}}D^{-4}\right) \leq CAhB^{-\frac{11}{2}}, \qquad \text{choosing } D = \frac{B}{2}.\end{aligned} \tag{2.24}$$

Since we assumed that Γ is bounded away from ∂S we have that I^0, I^1_i, $I^2_{i,j}$ remain bounded for x in Γ. Accordingly, we conclude that

$$\left|\tilde{N}u(x) - \int_\Gamma N(x,y)u(y)dy\right| \leq CAhB^{-\frac{11}{2}}, \tag{2.25}$$

for x in Γ_n such that $d(x) \geq B$.

Conclusion: Assume that u is in $C^3(W)$ while behaving at the boundary $\partial\Gamma$ as indicated by (2.5). If $\int_\Gamma N(x,y)u(y)dy$ is computed based on the method derived from equation (2.16), and if x is a fixed point on the grid Γ_n sufficiently far from $\partial\Gamma$, this method is of order $\mathcal{O}(h)$. This is verified numerically on an example in Section 2.3.

2.2.3. Boundary estimates

In this section we estimate the difference between the discrete sum and finite differences (2.16) and the continuous integrals and derivatives given by (2.15), if x is close the edge $\partial\Gamma$. Our first task is to determine the constant B introduced in (2.20) which we said depends only on the geometry of Γ. Fix δ in $(0,1)$ and set $R = d(x)^{1-\delta}$, if $d(x) < 1$. B is chosen small enough such that for all x in Γ such that $d(x) \leq B$ the projection of x on $\partial\Gamma$ is well defined and, in the disk centered at x and radius $R = d(x)^{1-\delta}$, $\partial\Gamma$ appears only as the perturbation of order R^2 of a line segment.

Case 3: y is away from x, $|y-x| \geq R$ but $d(x) \leq B$

In that case the argument from case 1 can be repeated to find in the end

$$\left| \int_{y\in S,\, R\leq|y-x|} N(x,y)\tilde{V}(y)dy \quad - \sum_{y\in S_n,\, R\leq|y-x|} N(x,y)\tilde{V}(y)h^2 \right| \leq ChAd(x)^{-\frac{3}{2}}R^{-4}. \quad (2.26)$$

Case 4: y is near x, $|y-x| \leq R$ and $d(x) \leq B$

We switch to a local coordinate system centered at x and we set $\rho = |x-y|$. By Taylor's formula

$$|\tilde{V}(y)| \leq C\rho^2 |\nabla\nabla u(x + s_1(y-x))|, \qquad |\nabla\tilde{V}(y)| \leq C\rho |\nabla\nabla u(x + s_2(y-x))|,$$

where $\nabla\nabla$ stands for the Hessian, and s_1, s_2 are in $(0,1)$. Referring to Fig. 2.1 we think of the line through x and its projection on $\partial\Gamma$ as the vertical axis and the line through x perpendicular to that first line the horizontal axis. ρ, θ will designate the polar coordinates in this local coordinate system. If y is in the upper part $D^+(x,R)$ of the disk $D(x,R)$ centered at x and of radius R then $d(x + s(y-x)) \geq Cd(x)$ thus,

$$|\tilde{V}(y)| \leq CA\rho^2 d(x)^{-\frac{3}{2}}, \quad |\nabla\tilde{V}(y)| \leq CA\rho d(x)^{-\frac{3}{2}}, \qquad \forall y \in D^+(x,R),$$

thus the difference

$$\int_{y\in S,\, y\in D^+(x,R)} N(x,y)\tilde{V}(y)dy \quad - \sum_{y\in S_n, h<|y-x|, y\in D^+(x,R)} N(x,y)\tilde{V}(y)h^2 \quad (2.27)$$

is of order

$$\sum_{y\in S_n, h<|y-x|, y\in D^+(x,R)} CAh^3\rho^{-2}d(x)^{-\frac{3}{2}},$$

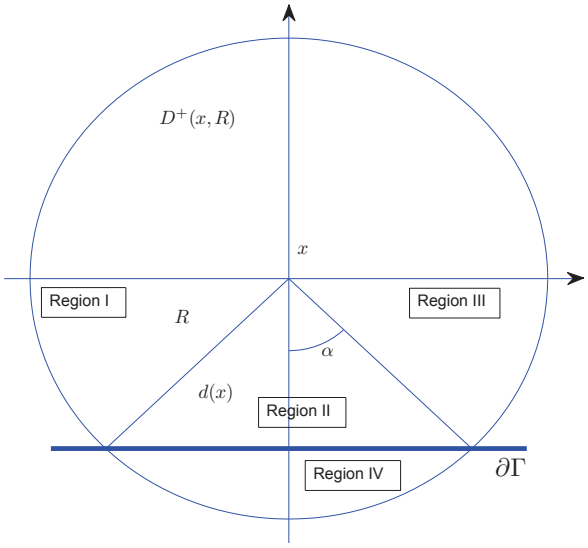

Fig. 2.1. A sketch of x near $\partial\Gamma$. Here $R = d(x)^{1-\delta}$ is small enough for $\partial\Gamma$ to be an $\mathcal{O}(R^2)$ perturbation of a line segment in $D(x,R)$.

which is less than

$$CAhd(x)^{-\frac{3}{2}}\int_h^R \rho^{-1}d\rho \leq CAh|\ln h|d(x)^{-\frac{3}{2}}. \tag{2.28}$$

We set $D^-(x,R) = D(x,R)\setminus D^+(x,R)$. Estimates for y in $D^-(x,R)$ are more delicate: they require using the local first order geometry near x and the following formula, valid if $0 < C_1 < C_2 < 1$,

$$\int_{C_1}^{C_2}\frac{d\rho'}{\rho'(1-\rho')^{\frac{3}{2}}} = -2\,\frac{1}{\sqrt{1-C_1}} + 2\,\frac{1}{\sqrt{1-C_2}} + \ln\left(\frac{\left(1-\sqrt{1-C_2}\right)\left(\sqrt{1-C_1}+1\right)}{\left(1-\sqrt{1-C_1}\right)\left(\sqrt{1-C_2}+1\right)}\right). \tag{2.29}$$

From examining the geometry of $D^-(x,R)$ we note that for y in that region and s in $(0,1)$

$$d(x+s(y-x)) \geq Cd(y) \geq C(d(x)-\rho\cos\theta).$$

To estimate the difference

$$\int_{y\in S,\, y\in D^-(x,R)} N(x,y)\tilde{V}(y)dy \quad - \sum_{y\in S_n, h<|y-x|, y\in D^-(x,R)} N(x,y)\tilde{V}(y)h^2, \tag{2.30}$$

we split $D^-(x,R)$ as indicated in Fig. 2.1. If y is in region I or III, the difference (2.30) for y in region I or III is bounded by

$$CAh\int_\alpha^{\frac{\pi}{2}}\int_h^R \frac{d\rho d\theta}{\rho(d(x)-\rho\cos\theta)^{\frac{3}{2}}}.$$

Setting $\rho' = \rho\cos\theta d(x)^{-1}$ and using formula (2.29), this previous integral is less than

$$CAh|\ln h|d(x)^{-\frac{3}{2}} + CAhd(x)^{-\frac{3}{2}}\int_\alpha^{\frac{\pi}{2}}(1-Rd(x)^{-1}\cos\theta)^{-\frac{1}{2}}d\theta. \tag{2.31}$$

This last integrand is unbounded since $\cos\alpha = d(x)^\delta$ and $Rd(x)^{-1} = d(x)^{-\delta}$, but the resulting integral is bounded since $\int_0^1 v^{-\frac{1}{2}}dv$ is convergent.

The geometry of region II is different. Notice that if $d(x) = h$ region II is empty; since x is in Γ_n, if region II is non empty then $d(x) \geq 2h$ so $d(x) - h \geq h$. The difference (2.30) in region II is less than

$$CAh\int_0^\alpha \int_{\frac{h}{\cos\theta}}^{\frac{d(x)-h}{\cos\theta}} \frac{d\rho d\theta}{\rho(d(x)-\rho\cos\theta)^{\frac{3}{2}}}.$$

Setting $\rho' = \rho\cos\theta d(x)^{-1}$ in the integral above we obtain

$$CAhd(x)^{-\frac{3}{2}}\int_0^\alpha \int_{\frac{h}{d(x)}}^{(1-\frac{h}{d(x)})} \frac{d\rho' d\theta}{\rho'(1-\rho')^{\frac{3}{2}}}.$$

Now using formula (2.29) we see that the previous expression is less than

$$CA(h|\ln h|d(x)^{-\frac{3}{2}} + h^{\frac{1}{2}}d(x)^{-1}). \tag{2.32}$$

In region IV, which lies outside Γ, $\rho \geq d(x)$ and $u(y) = 0$ so that

$$|\tilde{V}(y)| \leq Ad(x)^{\frac{1}{2}} + CAd(x)^{-\frac{1}{2}}\rho + CAd(x)^{-\frac{3}{2}}\rho^2,$$
$$|\nabla\tilde{V}(y)| \leq CAd(x)^{-\frac{1}{2}} + CAd(x)^{-\frac{3}{2}}\rho,$$

so that the difference (2.30) for y in region IV is bounded by

$$CAh\int_{d(x)}^{R}(d(x)^{\frac{1}{2}}\rho^{-4}+d(x)^{-\frac{1}{2}}\rho^{-3}+d(x)^{-\frac{3}{2}}\rho^{-2})\rho d\rho,$$

which is less than

$$CAhd(x)^{-\frac{3}{2}}|\ln d(x)|. \tag{2.33}$$

To estimate the difference

$$\sum_{y\in S_n,0<|y-x|<C} N(x,y)(\tilde{V}(y)-\tilde{U}(y))h^2,$$

we will use the fact that Γ is strictly included in S and that x is one of the grid points in Γ_n. We take C to be smaller than $1/\sqrt{2}$ times the distance from Γ to ∂S: the set of points $\{y\in S_n, 0<|y-x|<C\}$ is then symmetric about each of the two lines passing through x and parallel to the x_1 or x_2 axis. Accordingly

$$\begin{aligned}&\sum_{y\in S_n,0<|y-x|<C} N(x,y)(\tilde{V}(y)-\tilde{U}(y))h^2\\ =&-\frac{1}{2}\sum_{i=1}^{2}(\widetilde{\partial_i}(x)-\partial_i u(x))h^2\sum_{y\in S_n,0<|y-x|<C} N(x,y)(y_i-x_i)\end{aligned}$$

is zero simply because

$$\sum_{y\in S_n,0<|y-x|<C} N(x,y)(y_i-x_i)=0,$$

due to symmetries, and we conclude that

$$\left|\sum_{y\in S_n,y\neq x} N(x,y)(\tilde{V}(y)-\tilde{U}(y))h^2\right|\leq CAhd(x)^{-\frac{3}{2}}. \tag{2.34}$$

Since we assumed that Γ is bounded away from ∂S we have that I^0, I_i^1, $I_{i,j}^2$ remain bounded for x in Γ. Combining estimates (2.25), (2.26), (2.28), (2.31), (2.32), (2.33), (2.34), we conclude that

$$\begin{aligned}&\left|\tilde{N}u(x)-\int_\Gamma N(x,y)u(y)dy\right|\\ \leq&CA(h|\ln h|d(x)^{-\frac{3}{2}}+hd(x)^{-\frac{3}{2}-4(1-\delta)}+hd(x)^{-\frac{3}{2}}|\ln d(x)|+h^{\frac{1}{2}}d(x)^{-1}),\end{aligned} \tag{2.35}$$

where δ is fixed in $(0,1)$, C is constant depending only on δ, the geometry of $\partial\Gamma$ and its distance to ∂S, x is in Γ_n, u is in $C^3(\Gamma)$, and A was defined in (2.5).

2.2.4. Numerical convergence of eigenvectors

Proposition 2.1. *Let u be in $C^3(\Gamma)$ such that there is a positive constant A such that for all x in Γ*

$$|D^\alpha u(x)|\leq Ad(x)^{\frac{1}{2}-|\alpha|},\qquad 0\leq|\alpha|\leq 3.$$

The following estimate holds

$$\left|\int_\Gamma\int_\Gamma N(x,y)u(y)u(x)dydx - \sum_{x\in\Gamma_n} h^2(\tilde{N}u(x))u(x)\right| \leq CA^2h^{\frac{1}{2}}, \tag{2.36}$$

where C is a constant depending only on the geometry of $\partial\Gamma$.

Proof. By the triangle inequality

$$\left|\int_\Gamma\int_\Gamma N(x,y)u(y)u(x)dydx - \sum_{x\in\Gamma_n} h^2(\tilde{N}u(x))u(x)\right| \leq E_1 + E_2,$$

where

$$E_1 = \left|\int_\Gamma\int_\Gamma N(x,y)u(y)u(x)dydx - \sum_{x\in\Gamma_n} h^2\int_\Gamma N(x,y)u(y)dy \quad u(x)\right|,$$
$$E_2 = \left|\sum_{x\in\Gamma_n} h^2u(x)\Big(\tilde{N}u(x) - \int_\Gamma N(x,y)u(y)dy\Big)\right|.$$

We first estimate E_1. Since $|u(x)| \leq Ad(x)^{\frac{1}{2}}$ and $|\nabla u(x)| \leq Ad(x)^{-\frac{1}{2}}$, due to the properties of the singular integral operator $\mathcal{N}$ we may write the following estimates for $\mathcal{N}u$,

$$\left|\int_\Gamma N(x,y)u(y)dy\right| \leq CAd(x)^{-\frac{1}{2}}, \qquad \left|\nabla_x\int_\Gamma N(x,y)u(y)dy\right| \leq CAd(x)^{-\frac{3}{2}}.$$

Thus

$$\left|\nabla_x\left(\int_\Gamma N(x,y)u(y)dy \quad u(x)\right)\right| \leq CA^2d(x)^{-1}$$

and using one more time inequality (2.21) we find that

$$E_1 \leq \sum_{x\in\Gamma_n} CA^2h^3d(x)^{-1} \leq CA^2h\int_h^C t^{-1}dt \leq CA^2h|\ln h|.$$

We now proceed to estimate E_2. This is straightforward thanks to estimate (2.35)

$$\begin{aligned}
E_2 \leq& \sum_{x\in\Gamma_n} Ch^2A^2(h|\ln h|d(x)^{-1} + hd(x)^{-1-4(1-\delta)} + hd(x)^{-1}|\ln d(x)| + h^{\frac{1}{2}}d(x)^{-\frac{1}{2}})\\
\leq& CA^2\int_h^C (h|\ln h|t^{-1} + ht^{-1-4(1-\delta)} + ht^{-1}|\ln d(x)| + h^{\frac{1}{2}}t^{-\frac{1}{2}})dt\\
\leq& CA^2h^{\frac{1}{2}}, \text{ if } \delta \text{ is in } \left(\frac{7}{8},1\right).
\end{aligned}$$

Note that this latter constant C depends on the choice of δ. Estimate (2.36) results from combining the estimates for E_1 and for E_2. □

Proposition 2.2. *Fix $A > 1$ and denote $\mathcal{R}$ the subset of functions u in $C^3(\Gamma)$ such that*

$$\int_\Gamma u^2 = 1 \text{ and } \forall x\in\Gamma,\ |D^\alpha u(x)| \leq Ad(x)^{\frac{1}{2}-|\alpha|}, \qquad \text{where} \quad 0 \leq |\alpha| \leq 3.$$

Choose A to be large enough for $\mathcal{R}$ to contain the eigenfunction u_1 defined in (2.4). *The infinimum*

$$\inf_{u\in\mathcal{R}} \frac{\sum_{x\in\Gamma_n} h^2(\tilde{N}u(x))u(x)}{\sum_{x\in\Gamma_n} h^2u^2(x)}$$

converges to the first eigenvalue γ_1. Moreover we have the following estimate for the rate of convergence

$$\left|\gamma_1 - \inf_{u\in\mathcal{R}} \frac{\sum_{x\in\Gamma_n} h^2(\tilde{N}u(x))u(x)}{\sum_{x\in\Gamma_n} h^2u^2(x)}\right| \leq CA^4h^{\frac{1}{2}},$$

where C is a constant depending only on the geometry of $\partial\Gamma$.

Proof. Repeating the use of techniques shown earlier in this paper it can be proved that for all u in $\mathcal{R}$

$$\left|1 - \sum_{x\in\Gamma_n} h^2u^2(x)\right| \leq CA^2h. \tag{2.37}$$

In particular $\sum_{x\in\Gamma_n} h^2u^2(x) \geq 1/2$ if h is small enough. Applying the triangle inequality

$$\left|\int_\Gamma (\mathcal{N}u)(x)u(x)dx - \frac{\sum_{x\in\Gamma_n} h^2(\tilde{N}u(x))u(x)}{\sum_{x\in\Gamma_n} h^2u^2(x)}\right| \leq E_3 + E_4,$$

where

$$E_3 = \int_\Gamma (\mathcal{N}u)(x)u(x)dx \left|1 - \frac{1}{\sum_{x\in\Gamma_n} h^2u^2(x)}\right|,$$

$$E_4 = \frac{1}{\sum_{x\in\Gamma_n} h^2u^2(x)} \left|\int_\Gamma (\mathcal{N}u)(x)u(x)dx - \sum_{x\in\Gamma_n} h^2(\tilde{N}u(x))u(x)\right|.$$

Using (2.36) and (2.37) we find that $E_3 \leq CA^4h$ and $E_4 \leq CA^2h^{\frac{1}{2}}$. Now, since u is in $\tilde{H}^{\frac{1}{2}}(\Gamma)$ and $\int_\Gamma u^2 = 1$, we have that $\int_\Gamma (\mathcal{N}u)(x)u(x)dx \geq \gamma_1$. It follows that

$$\frac{\sum_{x\in\Gamma_n} h^2(\tilde{N}u(x))u(x)}{\sum_{x\in\Gamma_n} h^2u^2(x)} \geq \gamma_1 - CA^4h^{\frac{1}{2}},$$

for all u in $\mathcal{R}$. Since the vector u_1 is in $\mathcal{R}$ we must have

$$\frac{\sum_{x\in\Gamma_n} h^2(\tilde{N}u_1(x))u_1(x)}{\sum_{x\in\Gamma_n} h^2u_1^2(x)} \leq \gamma_1 + CA^4h^{\frac{1}{2}}.$$

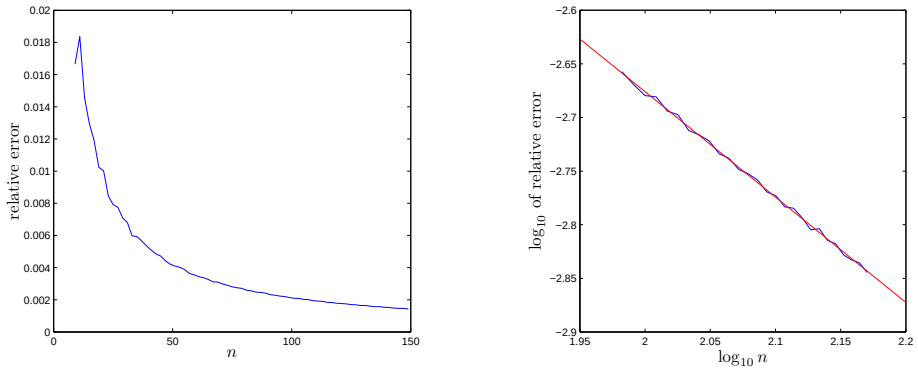

Fig. 2.2. Left: numerical error in computing the hypersingular integral (2.38) against n. $(n-1)^2$ collocation points were placed on the square S, but only those in Γ_n are used, see (2.10). Right: a log log rendition of the same data. The slope for the best linear fit, which appears in red is -0.99.

The previous two inequalities demonstrate that estimate (2.37) must hold.

Note: In practice a stronger convergence rate than that suggested by estimate (2.37) is achieved. We will show further in this paper that the observed rate is rather of order $\mathcal{O}(h|\ln h|)$, and in Appendix we show how estimates (2.36) and (2.37) can be improved to find $CA^4h^{\frac{2}{3}}|\ln h|$ as a final bound in (2.37).

2.3. Verification of the previous error estimates on a hypersingular integral whose exact value is known

We can evaluate in closed form the following hypersingular integral, where the unit disk centered at the origin is denoted $D(0,1)$,

$$\int_{D(0,1)} N(0,y)\sqrt{1-|y|^2}dy \tag{2.38}$$

by switching to polar coordinates and using the limiting process indicated in (2.9). The exact value is $\pi/4$. We then apply our numerical method given by (2.16) with the specific settings $\Gamma = D(0,1)$, $u(y) = \sqrt{1-|y|^2}$. Note that $u(y)$ is zero for y on $\partial\Gamma$ and $u(y) \sim d(y,\partial\Gamma)^{\frac{1}{2}}$ as y approaches $\partial\Gamma$ while remaining in Γ, just as the solution to (2.3). According to Section 2.2.2, the error incurred in our numerical method should be of order $\mathcal{O}(h)$. We show in Fig. 2.2 that this expected error is indeed confirmed by this computation.

2.4. Numerical solution to eigenvalue problem (2.1)

In this section we will present two sets of results on the numerical solution to eigenvalue problem (2.1). The first set is obtained by application of a finite element method to an adequately adjusted version of Eqs. (2.1). The second set is obtained by application of our numerical method introduced in Section 2.1 to integral equation (2.3).

To solve eigenvalue problem (2.1) by a finite elements method, we first recast it in the upper half space. Let $\mathbb{R}^{3+}$ be the upper half space defined by the equation $x_3 > 0$. We define the functional space $\mathcal{L}^+$ to be the closure for the norm $(\int_{\mathbb{R}^{3+}} |\nabla u|^2)^{\frac{1}{2}}$ of the space of scalar functions in $H^1(\mathbb{R}^{3+})$ with bounded support. We denote $\mathcal{L}_0^+$ the closed subspace of functions g in $\mathcal{L}^+$

such that g is zero in $\{x_3 = 0\} \setminus \overline{\Gamma}$. It was shown in [19] that f is in $\mathcal{L}$ and satisfies (2.1) if and only if the restriction of f to $\mathbb{R}^{3+}$ is in $\mathcal{L}_0^+$ and satisfies

$$\Delta f = 0, \qquad \text{in } \mathbb{R}^{3+}, \tag{2.39a}$$

$$\partial_n f = 2\gamma f, \quad \text{on } \Gamma. \tag{2.39b}$$

Next we introduce a bounded computational domain Ω defined by $x_3 > 0, \quad |x| < R$: we will define an approximation $\tilde{f}$ to f in Ω. On the portion of $\partial\Omega$ defined by $(\partial\Omega \cap \{x : x_3 = 0\}) \setminus \Gamma$, the boundary condition is imposed by the definition of the functional space $\mathcal{L}_0^+$, that is, $\tilde{f} = 0$. For the portion of $\partial\Omega$ defined by $\partial\Omega \cap \{x : |x| = R\})$, since we can derive the integral representation for f solution to (2.1)

$$f(x) = -\int_\Gamma \partial_{n(y)} G[f(y)]dy, \tag{2.40}$$

and since the estimate at infinity $\partial_{n(y)} G = \mathcal{O}(R^{-2})$ holds, we impose for $\tilde{f}$ the Robin condition

$$2R^{-1}\tilde{f} + \partial_r \tilde{f} = 0.$$

This is an $\mathcal{O}(R^{-4})$ accurate approximation. In Fig. 2.3 we indicate the computed value of γ the first eigenvalue for the problem

$$\Delta\tilde{f} = 0, \qquad \text{in } \Omega, \tag{2.41a}$$

$$\partial_n \tilde{f} = 2\gamma\tilde{f}, \qquad \text{on } \Gamma, \tag{2.41b}$$

$$\tilde{f} = 0, \qquad \text{on } (\partial\Omega \cap \{x : x_3 = 0\}) \setminus \Gamma, \tag{2.41c}$$

$$2R^{-1}\tilde{f} + \partial_r \tilde{f} = 0, \quad \text{on } \partial\Omega \cap \{x : |x| = R\}, \tag{2.41d}$$

$\tilde{f}$ was obtained by use of a finite element package. In the particular numerical example illustrated in Fig. 2.3, Γ is again the ellipse $x_1^2 + (x_2/.6)^2 \leq 1$ in the plane $x_3 = 0$. The number of degrees of freedom for the finite element method is given by n^2; n is borne out on the horizontal axis. These numbers are very large and require pre conditioning prior to proceeding to the numerical search for the first eigenvalue. This method seems to be converging, but, due to the introduction of the artificial boundary condition on $\partial\Omega \cap \{x : |x| = R\}$, it is far from clear how well the eigenvalue γ for (2.1) is approximated. Fig. 2.4 shows the meshing for the domain Ω in case of 5139 degrees of freedom. Note the clustering of edges near Γ. The finite element package is capable through mesh refinements to further cluster points near Γ as the number of degrees of freedom increases. Ultimately we are led to conclude based on Fig. 2.3 that the best approximation for γ is somewhere close to 1.34 or 1.35. Further increasing the number of degrees of freedom n^2 leads to prohibitively large matrices whose conditionings are too poor for the eigenvalue search to be productive.

In a second step we compute the eigenvalue γ for (2.1) following our approximation scheme (2.16). Fig. 2.5 shows values for γ_n, the computed value of γ where $(n-1)^2$ collocation points were placed on the square S, but only those in Γ_n are used, see (2.10). We also produce in Fig. 2.5 a log log rendition of the numerical error $|\gamma_{n+1} - \gamma_n| / \log_{10} n$. The rationale for plotting this quantity is that

$$\text{if } \gamma_n = \gamma + Cn^{-1}\ln n + o(n^{-1}\ln n), \text{ then } \frac{\gamma_{n+1} - \gamma_n}{\ln n} = o(n^{-1}),$$

$$\text{if } \gamma_n = \gamma + Cn^{-1}\ln n + \mathcal{O}(n^{-2}\ln n), \text{ then } \frac{\gamma_{n+1} - \gamma_n}{\ln n} = \mathcal{O}(n^{-2}).$$

The slope for the best linear fit appears to be -2. This is consistent with the claim that the numerical method for the eigenvalue problem is $\mathcal{O}(h \ln h)$ accurate.

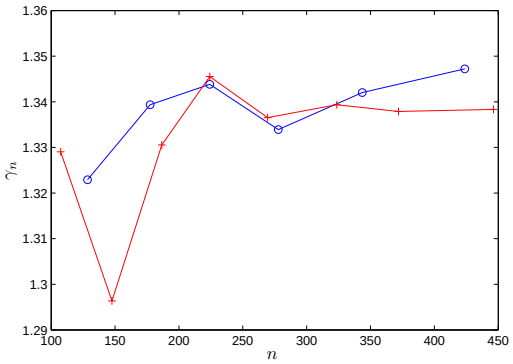

Fig. 2.3. Computed first eigenvalue γ_n for equations (2.41) using a finite element package. Γ is here the ellipse of equation $x_1^2 + (x_2/.6)^2 \leq 1$ in the plane $x_3 = 0$. The number of degrees of freedom is n^2. n is given on the horizontal axis and γ_n on the vertical axis. Blue circles: the radius R for domain truncation is 5. Red crosses: the radius R for domain truncation is 10.

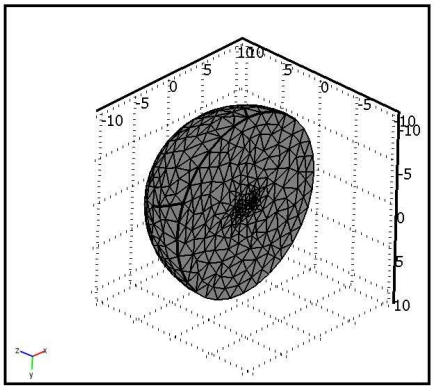

Fig. 2.4. Initial meshing of the computational domain Ω for 5139 degrees of freedom. Note how the mesh is finer near Γ.

We close this section by reporting that an attempt to use third derivatives for higher order regularization was ineffective due to deteriorating condition number. Additionally, clustering points near the boundary was also ineffective for two reasons: first, this is highly dependent on the geometry of Γ, and second, this leads to deteriorating condition number.

Finally let us make a remark on computational speed for integral equation method (2.6). Most of the computational time is spent on evaluating the coefficients of the matrix for the discretized problem. Assume now that n is fixed. We can first compute the coefficients of the matrix M_S for the discretized problem in the case $\Gamma = S$; then for any other geometry Γ, the coefficients of the matrix M_Γ for the respective discretized problem can be just sampled from the coefficients of M_S. From there finding the lowest eigenvalue for M_Γ typically takes about one second.

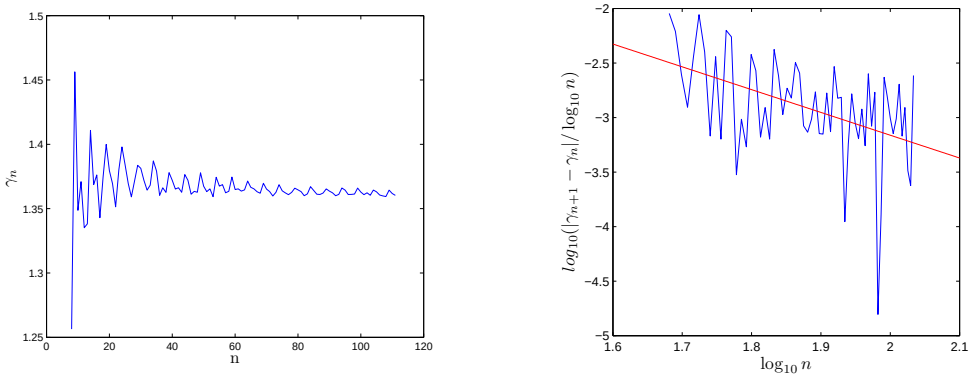

Fig. 2.5. Left: Computed value of γ_n the eigenvalue in (2.3) against n. $(n-1)^2$ collocation points were placed on the square S, but only those in Γ_n are used, see (2.10). In this example Γ is the ellipse $x_1^2 + (x_2/.6)^2 \leq 1$, $x_3 = 0$. Right: a log log rendition of the numerical error $|\gamma_{n+1} - \gamma_n|/\log_{10} n$. The slope for the best linear fit, which appears in red is -2.

3. The Eigenvalue Problem for a Crack in Free Space

3.1. Numerical method

In this section we will present two sets of results on the numerical solution to eigenvalue problem (1.2). First set is obtained by application of a finite element method to an adequately adjusted version of Eq. (1.2). The second set is obtained by application of our numerical method introduced in Section 2.1 to an integral equation formulation.

We take advantage one more time of symmetries to derive from (1.2) a PDE in the upper half space $\mathbb{R}^{3+}$. Full details of that derivation can be found in [19]. For vector fields u, v in $\mathbb{R}^{3+}$ of bounded support and whose gradient is square integrable, we introduce the bilinear product

$$B^+(u,v) = \int_{\mathbb{R}^{3+}} \lambda \operatorname{tr}(\nabla u)\operatorname{tr}(\nabla v) + 2\mu \operatorname{tr}(\epsilon(u)\epsilon(v)),$$

We define the functional space $\mathcal{V}^+$ to be the closure for the norm $B^+(u,u)^{\frac{1}{2}}$ of the space of vector fields in $H^1(\mathbb{R}^{3+})^3$ with bounded support. The natural norm on $\mathcal{V}^+$ is given by $B^+(u,u)^{\frac{1}{2}}$. In keeping with the notations used in [19], we introduce the closed subspace of $\mathcal{V}^+$:

$$\mathcal{V}^+_{0,2} = \Big\{ u \in \mathcal{V}^+ : u_2 = 0 \text{ on } \{x_3 = 0\} \text{ and } u_1 = \partial_3 u_3 = 0 \text{ on } \{x_3 = 0\} \setminus \overline{\Gamma} \Big\},$$

φ is in $\mathcal{V}_3$ and satisfies (1.2) if and only if the restriction of φ to $\mathbb{R}^{3+}$ is in $\mathcal{V}^+_{0,2}$ and satisfies

$$\mu\Delta\varphi + (\lambda+\mu)\nabla \operatorname{div} \varphi = 0, \qquad \text{in } \mathbb{R}^{3+} \tag{3.1a}$$
$$T_n\varphi \cdot e_3 = 0, \qquad \text{on } \Gamma, \tag{3.1b}$$
$$T_n\varphi \cdot e_1 = 2\beta\, \varphi \cdot e_1, \qquad \text{on } \Gamma, \tag{3.1c}$$
$$\varphi_2 = 0, \quad \text{on } \{x_3 = 0\}, \qquad \text{and} \qquad \varphi_1 = \partial_3\varphi_3 = 0, \quad \text{on } \{x_3 = 0\} \setminus \overline{\Gamma}. \tag{3.1d}$$

We use the same truncated computational domain Ω introduced in Section 2.3 where we solve

the PDE

$$\mu\Delta\tilde{\varphi} + (\lambda+\mu)\nabla\mathrm{div}\,\tilde{\varphi} = 0, \qquad \text{in } \Omega, \tag{3.2a}$$
$$T_n\tilde{\varphi}\cdot e_3 = 0, \qquad \text{on } \Gamma, \tag{3.2b}$$
$$T_n\tilde{\varphi}\cdot e_1 = 2\beta\,\tilde{\varphi}\cdot e_1, \qquad \text{on } \Gamma, \tag{3.2c}$$
$$\tilde{\varphi}_2 = 0, \quad \text{on } \{x_3=0\}, \qquad \text{and} \qquad \tilde{\varphi}_1 = \partial_3\tilde{\varphi}_3 = 0, \quad \text{on } (\{x_3=0\}\cap\Omega)\setminus\overline{\Gamma}, \tag{3.2d}$$
$$2R^{-1}\tilde{\varphi} + \partial_r\tilde{\varphi} = 0, \qquad \text{on } (\{|x|=R\}\cap\Omega). \tag{3.2e}$$

Approximating the solution to (3.1) by the solution to (3.1a)–(3.1d), the new boundary condition (3.2e) induces an $\mathcal{O}(R^{-4})$ error: we will explain why below.

The previous formulation is well suited to finite element element simulation. We now derive an integral equation formulation for problem (1.2). We start from Kelvin Green's tensor for linear elasticity in free space K given by,

$$K_{ij}(x,y) = \frac{1}{8\pi\mu(\lambda+2\mu)}((\lambda+\mu)\partial_{x_i}\,r\partial_{x_j}r + (\lambda+3\mu)\delta_{ij})\frac{1}{r}.$$

Defining the double layer potential by setting

$$\tilde{K}(x,y,n) = (T_{n(y)}K(x,y))^t, \tag{3.3}$$

we may express φ as the integral over Γ

$$\varphi(x) = -\int_\Gamma \tilde{K}(x,y,n)\varphi(y)dy. \tag{3.4}$$

In particular equation (3.4) shows that the boundary condition (3.2e) is satisfied by φ only up to an $\mathcal{O}(R^{-4})$ remainder. Eigenvalue problem (3.1a)–(3.1d) where the unknown φ is in $\mathcal{V}^+_{0,2}$ is equivalent to the following eigenvalue problem

$$\beta\varphi_1(x) = -T_{n(x)}\int_\Gamma \tilde{K}(x,y,n)\varphi_1(y)e_1dy\ \cdot e_1, \tag{3.5}$$

where the unknown φ_1 is in $\tilde{H}^{\frac{1}{2}}(\Gamma)$. To simplify notations we set $u = \varphi_1|_\Gamma$. Eq. (3.5) can be rewritten as

$$\beta\,u(x) = \int_\Gamma M_{11}(x,y)\,u(y)dy, \tag{3.6}$$

where u is in $\tilde{H}^{\frac{1}{2}}(\Gamma)$ and the integral is understood in the hypersingular sense. The explicit formula for $M_{11}(x,y)$ is given by

$$M_{11}(x,y) = -\frac{\mu}{4\pi}\,\frac{3\,\lambda\,(x_1-y_1)^2 + 2\,\mu\,\left((x_1-y_1)^2+(x_2-y_2)^2\right)}{(\lambda+2\,\mu)\left((x_1-y_1)^2+(x_2-y_2)^2\right)^{5/2}}. \tag{3.7}$$

In this case we apply a numerical scheme similar to that indicated by (2.16), safe for the six integrals I^0, I^1_i, $I^2_{i,j}$ which have to be replaced by, respectively,

$$J^0 := \int_S M_{11}(x,y)dy, \qquad J^1_i := \int_S (y_i-x_i)M_{11}(x,y)dy,$$
$$J^2_{i,j} := \int_S (y_i-x_i)(y_j-x_j)M_{11}(x,y)dy, \tag{3.8}$$

which have to be understood in the following generalized sense: for $x = (x_1, x_2)$ in Γ set $\mathbf{x} = (x_1, x_2, x_3)$, then

$$J^0 := -\lim_{x_3 \to 0} \int_S T_{n(x)} \tilde{K}(\mathbf{x}, y, n) dy, \qquad J_i^1 := -\lim_{x_3 \to 0} \int_S (y_i - x_i) T_{n(x)} \tilde{K}(\mathbf{x}, y, n) dy,$$
$$J_{i,j}^2 := -\lim_{x_3 \to 0} \int_S (y_i - x_i)(y_j - x_j) T_{n(x)} \tilde{K}(\mathbf{x}, y, n)) dy. \tag{3.9}$$

These integrals and limits can be evaluated in closed form. Formulas are provided in Appendix.

3.2. Numerical results

Our first set of results for computing the solution to (3.1) was produced by a finite element package. In this example Γ is still the ellipse $x_1^2 + (x_2/.6)^2 \leq 1, x_3 = 0$ and the values for the Lamé coefficients are $\lambda = 1$, $\mu = 2$. We plotted in Fig. 3.1 the computed first eigenvalue β_n for Eq. (3.2) using this finite element package against n, where the number of degrees of freedom is n^2. The numerical simulation was run for two values of the radius R of the computational domain. The method starts from a uniform mesh which is then locally refined based on local errors. Due to the refinement process the mesh exhibits significant clustering near Γ, as anticipated , and illustrated in Fig. 2.4. For low values of n, the numerical performance of the finite element package is now substantially less satisfactory than in the case relative to the Laplacian which was presented in Section 2.3. This is due to the fact that the present case involves solving for a vector field, and to more intricate boundary conditions, leading to poorly conditioned linear systems. For $R = 10$ low values of n do not lead to a solution; larger values required stringent pre conditioning of the discrete matrix for Eq. (3.2) before application of GMRES iterations. For values of n larger than 400, initial conditioning is just too poor: the numerical method fails.

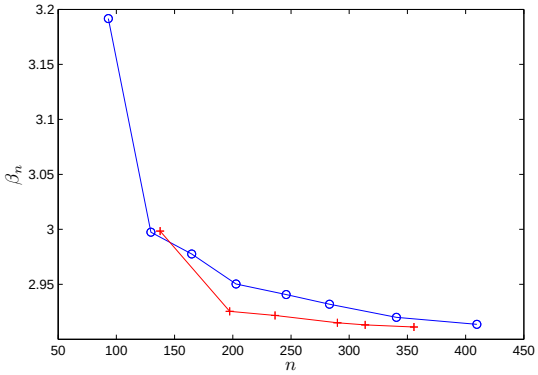

Fig. 3.1. Computed first eigenvalue β_n for Eq. (3.2) using a finite element package. The number of degrees of freedom is n^2. n is given on the horizontal axis and β_n on the vertical axis. Blue circles: the radius R for domain truncation is 5. Red crosses: the radius R for domain truncation is 10.

We now solve Eq. (3.1) by means of the integral formulation (3.6). To ease comparisons between methods, the geometry for Γ and the value for the Lamé coefficients are the same as in the previous case. We show:

- In Fig. 3.3, left: β_n, the computed values of β, the eigenvalue in (3.6), corresponding to $(n-1)^2$ collocation points placed on the square S (but only those in Γ_n are used, see (2.10))
- In Fig. 3.3, right: a log log rendition of the numerical error $|\beta_{n+1} - \beta_n|/\log_{10} n$. The slope for the best linear fit, which appears in red is, -2, as anticipated by our error analysis
- Fig. 3.4: left: a surface plot of φ_1, the first component of the eigenvector φ, on Γ, right: a contour line plot of the same quantity.
- Fig. 3.4, bottom: a cross section of the previous graph along the x_1 axis. The edge square root singularity is verified by fitting an expression in the form $(\sum_{i=1}^{4} a_i x_1^i)\sqrt{1-x_1^2}$ to match $u(x_1, 0)$.

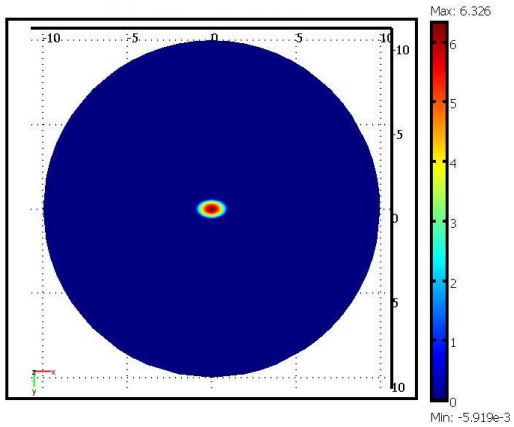

Fig. 3.2. Computed first eigenvector $\tilde{\varphi}$ for problem (3.2). Only $\tilde{\varphi}_1$ restricted to the the plane $x_3 = 0$ is shown. The solution does not change signs, as known theoretically from [19]. The computed value for β is 2.911175 for 126486 degrees of freedom if the radius R of the computational domain is set to 10.

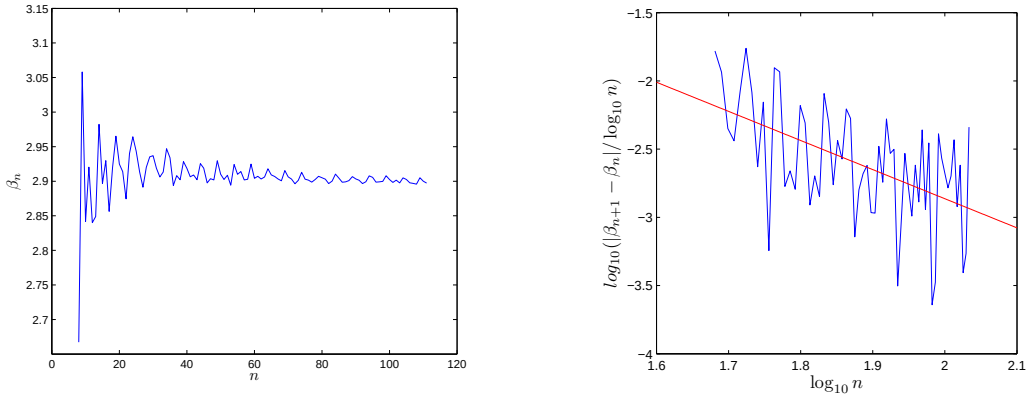

Fig. 3.3. Left: Computed value for β_n the eigenvalue in (3.6) against n. $(n-1)^2$ collocation points were placed on the square S, but only those in Γ_n are used, see (2.10). In this example Γ is the ellipse $x_1^2 + (x_2/.6)^2 \leq 1$, $x_3 = 0$. The Lamé coefficients are $\lambda = 1, \mu = 2$. Right: a log log rendition of the numerical error $|\beta_{n+1} - \beta_n|/\log_{10} n$. The slope for the best linear fit, which appears in red is -2.

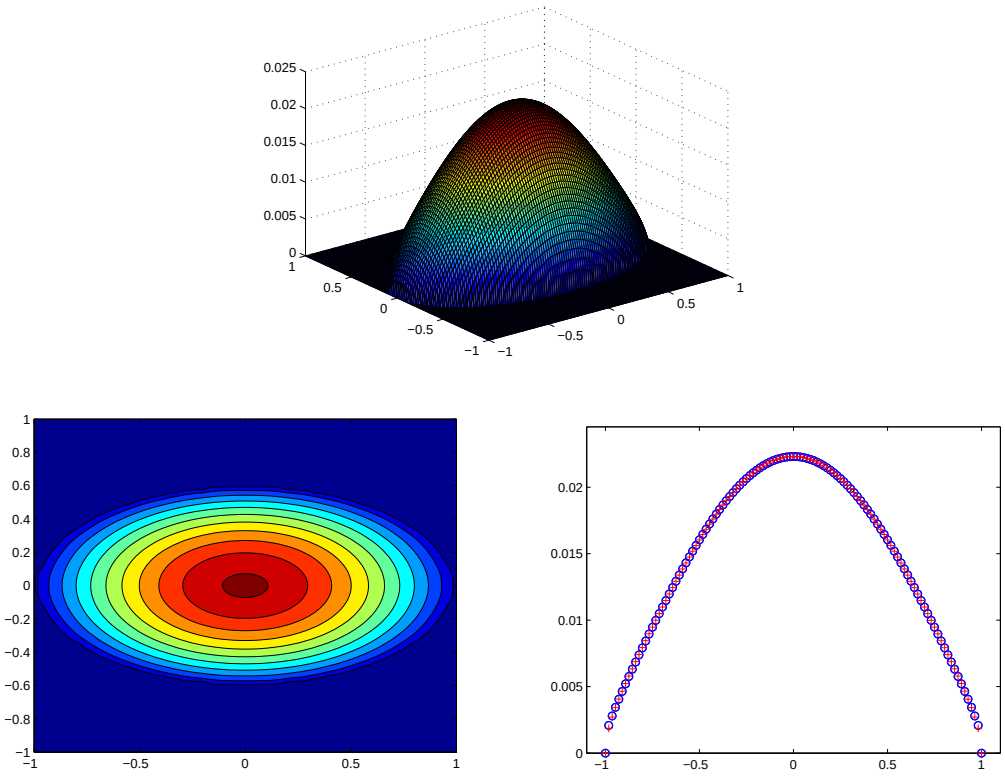

Fig. 3.4. Top Left: surface plot for u solution to (3.6). In this example Γ is the ellipse $x_1^2+(x_2/.6)^2 \leq 1$, $x_3 = 0$. The Lamé coefficients are $\lambda = 1, \mu = 2$. Top right: a contour plot for the same u. $(n-1)^2$ collocation points were placed on the square S, for $n = 111$, but only those in Γ_n are used, see (2.10). Bottom: a plot of the computed values of $u(x_1, 0)$: they appear as blue circles . The edge square root singularity is verified by fitting an expression in the form $(\sum_{i=1}^{4} a_i x_1^i)\sqrt{1-x_1^2}$ to match $u(x_1, 0)$. That best fit is plotted in red plus markers.

4. The Eigenvalue Problem for a Crack in Half Space

In this section we extend the study of the system (1.2) to the case of an elastic half space with traction free condition on the boundary. We start by constructing a functional space where problem (1.3) is well posed. For vector fields u, v in $H^1(\mathbb{R}^{3-} \setminus \Gamma)^3$ of bounded support we introduce the bilinear product

$$B^-(u,v) = \int_{\mathbb{R}^{3+}} \lambda \operatorname{tr}(\nabla u)\operatorname{tr}(\nabla v) + 2\mu \operatorname{tr}(\epsilon(u)\epsilon(v)),$$

We define the functional space $\mathcal{V}^-$ to be the closure under the norm $B^-(u,u)^{\frac{1}{2}}$ of the space of vector fields in $H^1(\mathbb{R}^{3-} \setminus \Gamma)^3$ of bounded support. We then pick $\mathcal{W}$, the following closed subspace of $\mathcal{V}^-$,

$$\mathcal{W} = \Big\{ u \in \mathcal{V}^- : [u \cdot n] = 0, [u \cdot t_2] = 0, \text{ across } \Gamma \Big\}.$$

We can now recast problem (1.3) in a more formal way:

$$\psi \in \mathcal{W}, \tag{4.1a}$$
$$\mu\Delta\psi + (\lambda+\mu)\nabla \mathrm{div}\,\psi = 0, \quad \text{in } \mathbb{R}^{3-} \setminus \overline{\Gamma}, \tag{4.1b}$$
$$T_{e_3}(\psi) = 0, \quad \text{on the surface } x_3 = 0, \tag{4.1c}$$
$$[T_n(\psi)] = 0, \quad \text{across } \Gamma \tag{4.1d}$$
$$T_n\psi \cdot t_1 = \beta\,[\psi \cdot t_1], \quad \text{across } \Gamma. \tag{4.1e}$$

Existence of eigenvectors can be shown by functional analysis techniques similar to those used in [19]. Next, we derive a boundary integral equation for problem (4.1). We need to use the second kind Green's tensor H relevant to problems in half space with traction free conditions on the surface. This tensor has been known for some time in the geophysics community, see the papers by Steketee [17] and Okada [13]. For a more mathematical approach to defining and computing H, as well as showing results on the uniqueness of H, see [18]. Eigenvalue problem (4.1) can be rewritten as

$$\beta[\psi(x)\cdot t_1] = \left(-T_{n(x)}\int_\Gamma H(x,y,n)[\psi(y)t]dy\right)\cdot t_1. \tag{4.2}$$

In order to solve integral equation (4.2) we need to know in closed form expressions for the components of the 3 by 3 by 3 tensor

$$\left(-T_{e_j(x)}H(x,y,n)e_k\right)\cdot e_i.$$

These closed form expressions are available in the public domain and appeared as a result of Okada's work [13]; they were also independently derived in a more mathematical way in [18]. We will underscore below the importance of this independent derivation. To handle singularities, our numerical method relies on the following splitting

$$\left(-T_{e_j(x)}H(x,y,n)e_k\right)\cdot e_i = \left(-T_{e_j(x)}\tilde{K}(x,y,n)e_k\right)\cdot e_i + R(x,y,n,i,j,k), \tag{4.3}$$

where $\tilde{K}$, the free space elasticity tensor of the second kind, is given by (3.3). Note that $R(x,y,n,i,j,k)$ is regular at $x=y$ and that the free space Green's tensor

$(-T_{e_j(x)}\tilde{K}(x,y,n)e_k)\cdot e_i$ is rotationally invariant. It follows that in local coordinates on Γ the same method as in free space, that is, the same method as in Section 3.1, can be applied to the singular part of integral equation (4.2). For $x \neq y$, the regular part $R(x,y,n,i,j,k)$ can be found by subtraction in (4.3), and the other two terms can be evaluated using available codes. We provide in Appendix formulas for $R(x,x,n,i,j,k)$: they result from the careful analysis performed in [18].

We now apply our integral equation method to problem (4.1), which is reduced to the integral equation (4.2). In the numerical example chosen to illustrate our method, Γ is obtained by the following linear transformations: start from the ellipse in the plane $x_3 = 0$ of equation $x_1^2 + (x_2/.6)^2 \leq 1$. Apply the rotation

$$\begin{pmatrix} \cos\theta & 0 & -\sin\theta \\ 0 & 1 & 0 \\ \sin\theta & 0 & -\cos\theta \end{pmatrix},$$

and then apply the vertical translation of vector $(0,0,d)$. The numerical values picked for θ and d are .7 and -.7 so that the coordinates of the highest point on Γ are $(\cos\theta, 0, d+\sin\theta)$, or

about, $(0.7648, 0, -0.0558)$, see Fig. 4.1. The Lamé coefficients are kept to be $\lambda = 1, \mu = 2$ as in the previous section. We show:

- in Fig. 4.2, left: β_n, the computed value of β, the eigenvalue relative to integral equation (4.2) and corresponding to $(n-1)^2$ collocation points placed on the square S (but only those in Γ_n are used, see (2.10))
- in Fig. 4.2, right: a log log rendition of the numerical error $|\beta_{n+1} - \beta_n| / \log_{10} n$. The slope for the best linear fit, which appears in red is -1.9.
- in Fig. 4.3, bottom: a cross section of the previous graph along the long axis of the ellipse Γ. The edge square root singularity is verified by fitting an expression in the form $(\sum_{i=1}^{4} a_i \tilde{x}_1^i)\sqrt{1-\tilde{x}_1^2}$ to match $u(\tilde{x}_1, 0)$, where $\tilde{x}_1$ is the first coordinate in the rotated frame. Note that in this half space case $u(\tilde{x}_1, 0)$, is not symmetric about zero.

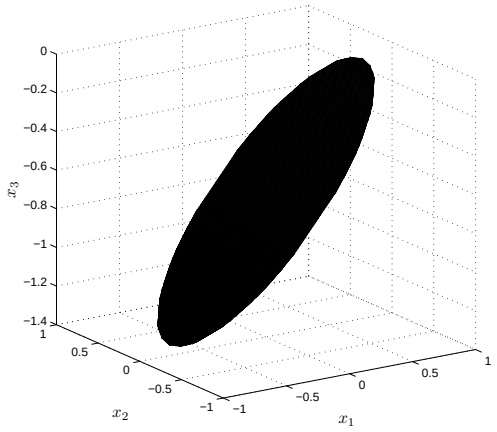

Fig. 4.1. A sketch of the fault Γ involved in the numerical calculation whose outputs are shown in Figs. 4.2 and 4.3. The highest point on Γ is $(\cos\theta, 0, d + \sin\theta)$, $d = -.7$, $\theta = .7$, or about, $(0.7648, 0, -0.0558)$.

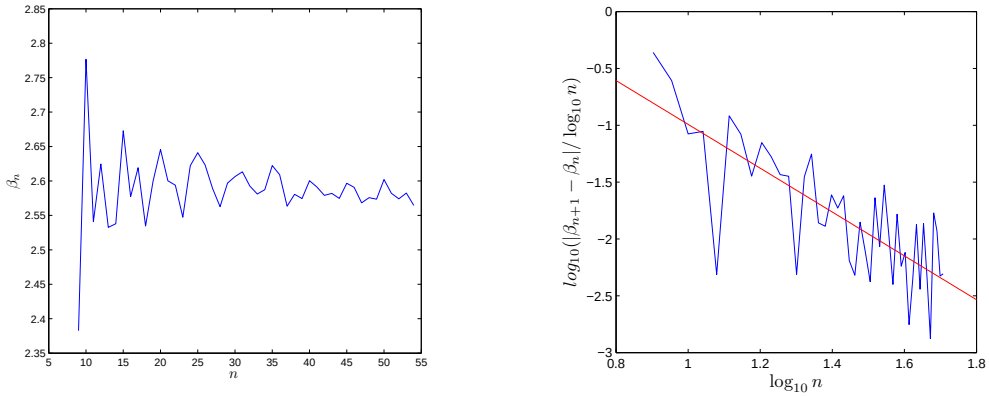

Fig. 4.2. Left: Computed value of β_n the eigenvalue in (4.2) against n. $(n-1)^2$ collocation points were placed on the square S (but only those in Γ_n are used, see (2.10)). In this example Γ is the ellipse sketched in Fig. 4.1. Right: a log log rendition of the numerical error $|\beta_{n+1} - \beta_n| / \log_{10} n$. The slope for the best linear fit, which appears in red, is -1.9.

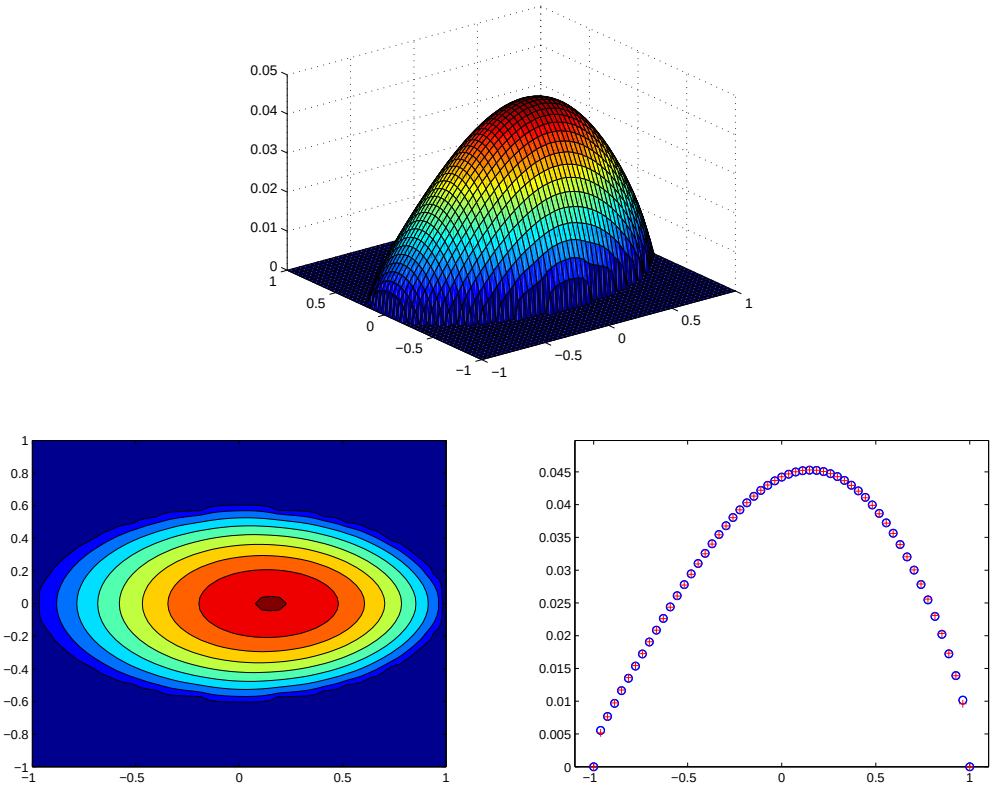

Fig. 4.3. Top Left: surface plot of $[\psi \cdot t_1]$, solution to (4.1), computed by solving integral equation (4.2). In this example Γ is the ellipse sketched in Fig. 4.1. Top right: a contour plot for $[\psi \cdot t_1]$. Bottom: a plot of the computed values of $[\psi \cdot t_1](\tilde{x}_1, 0)$: they appear as blue circles. Here $\tilde{x}_1$ is the first coordinate in the rotated frame. The edge square root singularity is verified by fitting an expression in the form $(\sum_{i=1}^{4} a_i \tilde{x}_1^i)\sqrt{1-\tilde{x}_1^2}$ to match $u(\tilde{x}_1, 0)$. Best fit is plotted in red plus markers.

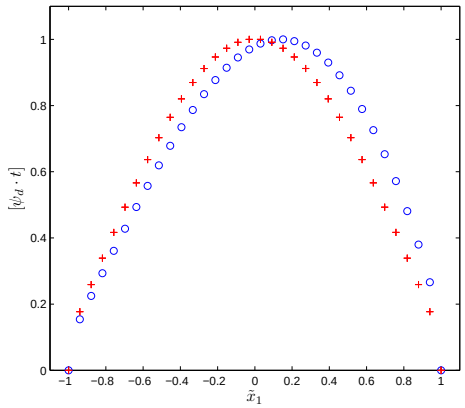

Fig. 4.4. Plots of $[\psi_d \cdot t_1]$ solution to solution to (4.1), computed by solving integral equation (4.2), against the local coordinate $\tilde{x}_1$ for the long axis of Γ. We picked four different values for the depth d, -.7, -5, -10, -50, while the incline angle θ remained fixed at .7. For $d = -.7$ the plot is done in blue circles. For $d = -5, -10, -50$, the corresponding three plots are indistinguishable at this scale. They are sketched using red crosses.

In our final set of numerical runs we seek to assess the effect of the depth d of the fault Γ. Denote ψ_d the normalized solution to (4.2) corresponding to the center of Γ being at $(0, 0, d)$, all the other parameters, the geometry of Γ, the angle θ, the coefficients λ and μ being kept the same as in the previous example. Since the difference between the free space Green's tensor $(-T_{e_j(x)}\tilde{K}(x, y, n)e_k) \cdot e_i$ and the half space Green's tensor $(-T_{e_j(x)}H(x, y, n)e_k) \cdot e_i$ is of order $\mathcal{O}(d^{-3})$, we expect ψ_d to converge to φ, solution to (3.1) at that same $\mathcal{O}(d^{-3})$ rate. Note that for a simpler two dimensional analog to this convergence problem, a complete mathematical and computational account of depth convergence properties was given in [7]. Fig. 4.4 shows graphs of $[\psi_d \cdot t]$ along the long axis of Γ for four values of d. Very rapid convergence in d is observed.

5. Conclusion

We have presented in this paper a novel numerical method for hypersingular integral equations on planar surfaces in space. We have applied this method to the numerical solution to an eigenvalue problem in linear elasticity which models the quasi static evolution of destabilized faults in free space or in half space. We observed that our numerical method is $\mathcal{O}(h \ln h)$ accurate, which is slightly better than the $\mathcal{O}(h^{\frac{2}{3}} \ln h)$ derived in our rigorous error analysis. In free space our method is better conditioned than those obtained from finite element packages and features an additional advantage: it is very fast once the Lamé coefficients λ and μ have been set and the matrix corresponding to the unit square geometry has been computed. This point is especially relevant to shape inverse problems for faults.

In half space our method still performs very well even for those faults which are very close to the top boundary. Note that finite element methods are particularly ill suited to that case.

It is worth mentioning another interesting application of the numerical method introduced in this paper. This application pertains to boundary value problems with prescribed forces on a crack. For the laplacian case this corresponds to solving the integral equation of the first kind

$$\int_\Gamma N(x, y)u(y) = f(x).$$

This could be done by first finding the m lowest eigenvalues and eigenvectors $v_1, \cdots, v_m$ for problem (2.3) and then projecting the forcing term f on the span of $v_1, \cdots, v_m$.

The prospect of extending the new computational method introduced in this study to the case of non planar faults is particularly interesting. We do not know at present whether the special quadrature rules introduced in this paper could still be helpful in that case; an approximation of the fault surface by contiguous triangles could possibly be more fruitful. Another line of research worth pursuing pertains to the generalization of this present study to fully dynamic problems. Formulas for Green's tensors in frequency or time regime relative to elasticity problems in half space have been known for some time in the isotropic case. They are referred to in the literature as Lamb's solutions, see [8]. Unfortunately these solutions are not entirely explicit; they involve integrals that have to be evaluated either numerically or asymptotically, and accordingly much work has been done in order to find efficient ways to formulate or evaluate Lamb's solutions, see [4] and [20].

6. Appendix

6.1. The integrals defined in (2.8)–(2.9) and in (3.8)–(3.9)

To avoid prohibitively lengthy formulas we introduce the following notations

$$\begin{aligned}
&u_1 = -1 - x_1, \qquad v_1 = 1 - x_1\\
&u_2 = -1 - x_2, \qquad v_2 = 1 - x_2\\
&p = \sqrt{u_1^2 + u_2^2}, \qquad q = \sqrt{v_1^2 + v_2^2}, \qquad r = \sqrt{u_1^2 + v_2^2}, \qquad s = \sqrt{v_1^2 + u_2^2}.
\end{aligned}$$

The six integrals I^0, I^1_i, $I^2_{i,j}$ are then given by

$$\begin{aligned}
I^0 &= \frac{1}{4\,\pi}\left(\frac{u_2}{u_1 p} + \frac{v_1}{v_2 q} + \frac{u_1}{p u_2} - \frac{v_1}{u_2 s} + \frac{v_2}{q v_1} - \frac{u_1}{v_2 r} - \frac{u_2}{s v_1} - \frac{v_2}{u_1 r}\right),\\
I^1_1 &= \frac{1}{4\,\pi}\,\ln\left(\frac{(u_2+p)\,(v_2+q)}{(u_2+s)\,(v_2+r)}\right), \qquad I^1_2 = \frac{1}{4\,\pi}\,\ln\left(\frac{(u_1+p)\,(v_1+q)}{(u_1+r)\,(v_1+s)}\right),\\
I^2_{1,1} &= \frac{1}{4\,\pi}\Big(-u_2\ln(u_1+p) + v_2\ln(u_1+r) + u_2\ln(v_1+s) - v_2\ln(v_1+q)\Big),\\
I^2_{2,2} &= \frac{1}{4\,\pi}\Big(-u_1\ln(u_2+p) + v_1\ln(u_2+s) + u_1\ln(v_2+r) - v_1\ln(v_2+q)\Big),\\
I^2_{1,2} &= \frac{1}{4\,\pi}\,(p+q-r-s)\,.
\end{aligned}$$

To give closed form solutions for the integrals defined in (3.8)–(3.9), we introduce the additional notations: a will stand for the function arcsinh and C will be the constant $(-\mu/4\pi(\lambda+2\mu))^{-1}$.

$$\begin{aligned}
CJ^0 &= \left(u_1(\frac{1}{pu_2} - \frac{1}{rv_2}) + v_1(\frac{1}{qv_2} - \frac{1}{sv_2})\right)(\frac{\lambda}{2} + \mu) + \left(u_2(\frac{1}{pu_1} - \frac{1}{sv_1}) + v_2(\frac{1}{qv_1} - \frac{1}{ru_1})\right)(\lambda + \mu)\\
CJ^1_1 &= \log\left(\frac{(v_2+q)(u_2+p)}{(v_2+r)(u_2+s)}\right)(\mu+\lambda) + \frac{\lambda}{2}\left(v_2(\frac{1}{q} - \frac{1}{r}) + u_2(\frac{1}{p} - \frac{1}{s})\right)\\
CJ^1_2 &= \log\left(\frac{(v_1+q)(u_1+p)}{(v_1+s)(u_1+r)}\right)(\mu + \frac{\lambda}{2}) + \frac{\lambda}{2}\left(v_1(\frac{1}{s} - \frac{1}{q}) + u_1(\frac{1}{r} - \frac{1}{p})\right)\\
CJ^2_{1,1} &= \left(\log(\frac{u_1+r}{v_1+q})v_2 + \log(\frac{u_1-p}{v_1-s})u_2\right)(\mu + \frac{3\lambda}{2}) + \left(u_1(\frac{u_2}{p} - \frac{v_2}{r}) + v_1(\frac{v_2}{q} - \frac{u_2}{s})\right)\frac{\lambda}{2}\\
CJ^2_{2,2} &= \left(\log(\frac{u_2+s}{v_2+q})v_1 + \log(\frac{u_2-p}{v_2-r})u_1\right)\mu + \left(u_2(\frac{v_1}{s} - \frac{u_1}{p}) + v_2(\frac{u_1}{r} - \frac{v_1}{q})\right)\frac{\lambda}{2}\\
CJ^2_{1,2} &= \left((\frac{1}{p} - \frac{1}{r})u_1^2 + (\frac{1}{q} - \frac{1}{s})v_1^2\right)(\mu + \frac{\lambda}{2}) + \left((\frac{1}{p} - \frac{1}{s})u_2^2 + (\frac{1}{q} - \frac{1}{r})v_2^2\right)(\mu + \lambda).
\end{aligned}$$

6.2. The regular tensor $R(x, x, n, i, j, k)$

$R(x, x, n, i, j, k)$ depends on x only through x_3. To simplify notations denote R_{ijk} for $R(x, x, n, i, j, k)$. We first notice the symmetry relation

$$R_{ijk} = R_{jik}.$$

The formulas for the entries of R are therefore reduced to

$$R_{111} = -\frac{1}{32}\frac{\left(7\,\lambda^2+9\,\mu\,\lambda+5\,\mu^2\right)n_1\mu}{{x_3}^3\pi\,\left(\lambda^2+3\,\mu\,\lambda+2\,\mu^2\right)}, \qquad R_{112} = -\frac{1}{32}\frac{\left(\lambda^2-\mu\,\lambda-\mu^2\right)n_2\mu}{{x_3}^3\pi\,\left(\lambda^2+3\,\mu\,\lambda+2\,\mu^2\right)},$$

$$R_{113} = -\frac{1}{8}\frac{\mu\,n_3\,(-\mu+\lambda)}{{x_3}^3\pi\,(\lambda+2\,\mu)}, \qquad R_{121} = -\frac{1}{32}\frac{\left(3\,\lambda^2+5\,\mu\,\lambda+3\,\mu^2\right)n_2\mu}{{x_3}^3\pi\,\left(\lambda^2+3\,\mu\,\lambda+2\,\mu^2\right)},$$

$$R_{122} = -\frac{1}{32}\frac{\left(3\,\lambda^2+5\,\mu\,\lambda+3\,\mu^2\right)n_1\mu}{{x_3}^3\pi\,\left(\lambda^2+3\,\mu\,\lambda+2\,\mu^2\right)},$$

$$R_{123} = 0, \qquad R_{131} = -\frac{1}{32}\frac{\mu\,n_3\,(10\,\mu+9\,\lambda)}{{x_3}^3\pi\,(\lambda+2\,\mu)},$$

$$R_{132} = 0, \qquad R_{133} = -\frac{1}{32}\frac{n_1\mu\,(10\,\mu+9\,\lambda)}{{x_3}^3\pi\,(\lambda+2\,\mu)},$$

$$R_{221} = -\frac{1}{32}\frac{\left(\lambda^2-\mu\,\lambda-\mu^2\right)n_1\mu}{{x_3}^3\pi\,\left(\lambda^2+3\,\mu\,\lambda+2\,\mu^2\right)}, \qquad R_{222} = -\frac{1}{32}\frac{\left(7\,\lambda^2+9\,\mu\,\lambda+5\,\mu^2\right)n_2\mu}{{x_3}^3\pi\,\left(\lambda^2+3\,\mu\,\lambda+2\,\mu^2\right)},$$

$$R_{223} = -\frac{1}{8}\frac{\mu\,n_3\,(-\mu+\lambda)}{{x_3}^3\pi\,(\lambda+2\,\mu)}, \qquad R_{231} = 0, \qquad R_{232} = -\frac{1}{32}\frac{\mu\,n_3\,(10\,\mu+9\,\lambda)}{{x_3}^3\pi\,(\lambda+2\,\mu)},$$

$$R_{233} = -\frac{1}{32}\frac{n_2\mu\,(10\,\mu+9\,\lambda)}{{x_3}^3\pi\,(\lambda+2\,\mu)}, \qquad R_{331} = -\frac{1}{8}\frac{(-\mu+\lambda)\,n_1\mu}{{x_3}^3\pi\,(\lambda+2\,\mu)}, \qquad R_{332} = -\frac{1}{8}\frac{(-\mu+\lambda)\,n_2\mu}{{x_3}^3\pi\,(\lambda+2\,\mu)},$$

$$R_{333} = -\frac{5}{4}\frac{\mu\,n_3\,(\lambda+\mu)}{{x_3}^3\pi\,(\lambda+2\,\mu)}.$$

6.3. Improved bounds for estimates (2.36) and (2.37)

The lowest order term in our error analysis is the $h^{1/2}d(x)^{-1}$ term in estimate (2.35). Recall that that term was derived by summing a bound on the gradient of $N(x,y)\tilde{V}(y)$ in Region II, which was sketched in Fig. 2.1 . An improved estimate can be performed by splitting Region II in two parts, II.a. and II.b., if $d(x) \geq h^\eta$ for some η in $(0,1)$ to be optimized later. In Region II.a. ρ will range from h to h^η and the other estimates are carried out in a similar fashion to find an error in the form $CAhd(x)^{-3/2}$. In Region II.b. ρ will range from $h^\eta/\cos\theta$ to $(d(x)-h)/\cos\theta$ and we use the following alternative estimates for $\tilde{V}$ and its gradient

$$|\tilde{V}(y)| \leq CA\rho \sup_{s\in(0,1)} |\nabla u(x+s(y-x))| + CA\rho^2 d(x)^{-\frac{3}{2}},$$

$$|\nabla\tilde{V}(y)| \leq CA \sup_{s\in(0,1)} |\nabla u(x+s(y-x))| + CA\rho d(x)^{-\frac{3}{2}}.$$

The error is bounded by

$$CAh\int_0^\alpha \int_{\frac{h^\eta}{\cos\theta}}^{\frac{d(x)-h}{\cos\theta}} \frac{d\rho d\theta}{\rho^2(d(x)-\rho\cos\theta)^{\frac{1}{2}}} + CAh|\ln h|d(x)^{-\frac{3}{2}},$$

which is bounded by $CAh^{1-\eta}d(x)^{-3/2}$. Thanks to this process we obtain a new form for estimate (2.35) which now appears as

$$CAh^{1-\eta}d(x)^{-\frac{3}{2}}1_{\{d(x)\geq h^\eta\}} + CAh^{\frac{1}{2}}d(x)^{-1}1_{\{h\leq d(x)\leq h^\eta\}},$$

in place of merely $CAh^{1/2}d(x)$. Multiplying by $h^2d(x)^{1/2}$ and summing for x in Γ_n we find this new improved term the bound

$$CAh^{1-\eta}\int_{h^\eta}^{C} t^{-1}dt + CAh^{\frac{1}{2}}\int_h^{h^\eta} t^{-\frac{1}{2}}dt,$$

which is in turn bounded by

$$CAh^{1-\eta}|\ln h| + CAh^{\frac{1}{2}+\frac{\eta}{2}}.$$

We now optimize for η in $(0,1)$. Since

$$\max_{\eta\in(0,1)} \min\{1-\eta, \frac{1}{2}+\frac{\eta}{2}\} = \frac{2}{3},$$

where the maximum is achieved for $\eta = 1/3$, the improved bound $CA^2h^{2/3}|\ln h|$ can be chosen for estimate (2.36). Subsequently the improved bound $CA^4h^{2/3}|\ln h|$ can be chosen for estimate (2.37).

Acknowledgments. Partial support for this work was provided by NSF grant DMS 0707421.

References

[1] H. Aochi, E. Fukuyama, and M. Matsumura, Spontaneous Rupture Propagation on a Non-planar Fault in 3-D Elastic Medium, *Pure Appl. Geophys.*, **157** (2000), 2003-2027.

[2] L. Badea, I. R. Ionescu, and S. Wolf, Schwarz method for earthquake source dynamics, *J. Comput. Phys.*, **227** (2008), 3824-3848.

[3] C. Dascalu, I. R. Ionescu, and M. Campillo, Fault finiteness and initiation of dynamic shear instability, *Earth Planet. Sc. Lett.*, **177** (2000), 163-176.

[4] G. P. Eatwell, J. A. Simmons, and J. R. Willis, A new representation for the dynamic green's tensor of an elastic half-space or layered medium, *Wave Motion*, **4** (1982), 53-73.

[5] K. L. Feigl and E. Dupré, RNGCHN: a program to calculate displacement components from dislocations in an elastic half-space with applications for modeling geodetic measurements of crustal deformation, *Computers & Geosciences*, **25** (1999) 695-704.

[6] G. C. Hsiao, E. Schnack, and W. L. Wendland, A hybrid coupled finite-boundary element method in elasticity, *Comput. Method. Appl. M.*, **173** (1999), 287-316.

[7] I. R. Ionescu, D. Volkov, Earth surface effects on active faults: an eigenvalue asymptotic analysis, *J Comput. Appl. Math.*, **220** (2008), 143-162.

[8] L. R. Johnson, Green's Function for Lamb's Problem, *Geophys. J. R. asfr. Soc.*, **37** (1974), 99-131.

[9] P. A. Martin, L. Paivarinta, and S. Rempel, A normal crack in an elastic half-space with stress-free surface, *Math. Method. Appl. Sci.*, **16** (1992), 563-579.

[10] P. A. Martin and F. J. Rizzo, On Boundary Integral Equations for Crack Problems, *Proceedings of the Royal Society of London. Series A, Mathematical and Physical Sciences*, **421**, 341-355.

[11] J. C. Nedelec, Acoustic and Electromagnetic Equations, Applied Mathematical Sciences 144, Springer.

[12] Z. Niu, W. L. Wendland, X. Wang, and H. Zhou, A semi-analytical algorithm for the evaluation of the nearly singular integrals in three-dimensional boundary element methods, *Comput. Method. Appl. M.*, **194** (2005) 1057-1074.

[13] Y. Okada, Internal deformation due to shear and tensile faults in a half-space, *Bulletin of the Seismological Society of America*, **82** (1992), 1018-1040.

[14] L. Pan, F. Rizzoa, and P. A. Martin, Some efficient boundary integral strategies for time-harmonic wave problems in an elastic halfspace, *Comput. Method. Appl. M.*, **164** (1998), 207-221

[15] E. P. Stephan, A boundary integral equation method for three-dimensional crack problems in elasticity, *Math. Method. Appl. Sci.*, **8** (1986), 609-623.

[16] E. P. Stephan, M. Maischak, and T. Tran, Domain Decomposition Algorithms for an Indefinite Hypersingular Integral Equation in Three Dimensions, *Domain Decomposition Methods in Science and Engineering XVII, Lect. Notes Comput. Sc.*, **60**, 647-655.

[17] J. A. Steketee, On Volterra's dislocations in a semi infinite elastic medium, *Can. J. Phys.*, **36** (1958), 192-205.

[18] D. Volkov, A double layer surface traction free Green's tensor, *SIAM J. Appl. Math.*, **69** (2009), 1438-1456.

[19] D. Volkov, An eigenvalue problem for elastic cracks in free space, *Math. Method. Appl. Sci.*, **33** (2010), 607-622.

[20] C. Y. Wang, and J. D. Achenbach, Lamb's problem for solids of general anisotropy, *Wave Motion*, **24** (1996), 227-242.

[21] W. L. Wendland, and E. P. Stephan, A hypersingular boundary integral method for two-dimensional screen and crack problems, *Arch. Ration. Mech. An.*, **112** (1990), 363-390.

[22] L. Ying, G. Biros, and D. Zorin, A high-order 3D boundary integral equation solver for elliptic PDEs in smooth domains, *J. Comput. Phys.*, **219** (2006), 247-275.